DOT/FAA/TC-24/35

Federal Aviation Administration
William J. Hughes Technical Center
Aviation Research Division
Atlantic City International Airport
New Jersey 08405

Investigation of Certification Considerations for Distributed Electric Propulsion (DEP) Aircraft

October 2024

Final report

U.S. Department of Transportation
Federal Aviation Administration

NOTICE

This document is disseminated under the sponsorship of the U.S. Department of Transportation in the interest of information exchange. The U.S. Government assumes no liability for the contents or use thereof. The U.S. Government does not endorse products or manufacturers. Trade or manufacturers' names appear herein solely because they are considered essential to the objective of this report. The findings and conclusions in this report are those of the author(s) and do not necessarily represent the views of the funding agency. This document does not constitute FAA policy. Consult the FAA sponsoring organization listed on the Technical Documentation page as to its use.

This report is available at the Federal Aviation Administration William J. Hughes Technical Center's Full-Text Technical Reports page: actlibrary.tc.faa.gov in Adobe Acrobat portable document format (PDF).

Technical Report Documentation Page

Form DOT F 1700.7 (8-72) Reproduction of completed page authorized

1. Report No.	2. Government Accession No.	3. Recipient's Catalog No.
DOT/FAA/TC-24/35		

4. Title and Subtitle	5. Report Date
Investigation of Certification Considerations for Distributed Electric Propulsion (DEP) Aircraft	October 2024
	6. Performing Organization Code

7. Author(s)	8. Performing Organization Report No.
R. McKillip, Jr., D. Wachspress	CDI Report 24-08

9. Performing Organization Name and Address	10. Work Unit No. (TRAIS)
Continuum Dynamics, Inc. 34 Lexington Ave. Ewing, NJ 08618	11. Contract or Grant No. 692M15-22-T-00019

12. Sponsoring Agency Name and Address	13. Type of Report and Period Covered
AAQ-610 Facilities & Grants FAA William J. Hughes Technical Center, Fourth Floor, Bldg 300 Atlantic City International Airport Atlantic City, NJ 08405	Draft Final 6/14/2022-7/31/2024
	14. Sponsoring Agency Code

15. Supplementary Notes

David Sizoo and Ross Schaller initiated and sponsored this project. It is part of a portfolio of research sponsored by the Flight Test Branch of the FAA's Aircraft Certification Line of Business. These projects have outcomes that enable Advanced Air Mobility Certification by identifying technical issues through direct experiments. This approach is used to enable policy and flight test techniques to safely certify new technology.

16. Abstract

Efforts from a multi-year investigation examining the use of estimation of remaining vehicle control power margins and external environmental disturbances for distributed electric propulsion (DEP) vehicles as a contributor for vehicle certification are described. This study combines simulation of DEP aircraft with experimental testing of representative models in the assessment of algorithms for determining remaining control power margins in real-time vehicle operation. Additionally, to provide a metric for the capability of the vehicle to accommodate operational disturbances and avoid loss of control in-flight (LOC-I) events. The Comprehensive Hierarchical Aeromechanics Rotorcraft Model (CHARM) analysis for aerodynamic interaction effects on the configurations was used to simulate and characterize vehicle response to disturbances and to applied control inputs throughout its flight envelope. The goal of the effort was to determine the viability of the methods to calculate remaining control power margins and disturbance intensities, and to assess the utility of the methods in safety monitoring of DEP flight operations for both piloted and uncrewed vehicles.

17. Key Words	18. Distribution Statement
Remaining control power, distributed electric propulsion, eVTOL aircraft, loss of control sensing	This document is available to the U.S. public through the National Technical Information Service (NTIS), Springfield, Virginia 22161. This document is also available from the Federal Aviation Administration William J. Hughes Technical Center at actlibrary.tc.faa.gov.

19. Security Classif. (of this report)	20. Security Classif. (of this page)	21. No. of Pages	19. Security Classif. (of this report)
Unclassified	Unclassified	61	Unclassified

Contents

Figures

Acronyms

Acronym	Definition
ATC	Air traffic control
CDI	Continuum Dynamics, Inc.
CETI	Control equivalence turbulence input
CHARM	Comprehensive Hierarchical Aeromechanics Rotorcraft Model
DEP	Distributed electric propulsion
DEPSim	DEP aircraft simulation
DOF	Degree of freedom
DOT	Department of Transportation
eVTOL	Electric vertical take-off and landing
FAA	Federal Aviation Administration
FCS	Flight control system
FlightCODE	Flight dynamics Computation of Ordinary Differential Equations
fps	feet per second
GA	General aviation
GPU	Graphics processing unit
IMU	Inertial measurement unit
KACY	Atlantic City International Airport
LOC	Loss of control
LOC-I	Loss of control in-flight
LpC	Lift plus cruise configuration
MATLAB	Matrix Laboratory
METAR	Meteorological aerodrome reports
METS	Mixer equivalent turbulence simulation
NASA	National Aeronautics and Space Administration
NDARC	NASA Design and Analysis of Rotorcraft
PIREP	Pilot report
PWM	Pulse Width Modulation
RCP	Remaining control power
SWaP	Size, weight and power
UAM	Urban air mobility
UAS	Unmanned aircraft system
UAV	Unmanned air vehicle

UDB5	UAV data board v5
VTOL	Vertical take-off and landing

Executive summary

A multi-year effort examining the definition and algorithmic computation of remaining control power (RCP) as a metric for assessment of potential loss of control (LOC) events is described. Algorithms for computing RCP were investigated through analysis, simulation, and testing on representative scaled vehicles. The vehicles required configurations that capture current design concepts in development within the distributed electric propulsion (DEP) vertical takeoff and landing (VTOL) space. These aircraft are characterized by multiple lifting rotors, which may articulate (possibly along with attached wings) and/or are augmented by additional propulsion units and other lifting surfaces. Many concepts provide redundant controls for safety enhancement, and all incorporate some form of feedback stabilization to aid flying qualities and provide disturbance rejection. Assessment of remaining control power, and its algorithmic computation, is challenged with this complexity. However, to be successful, it must be performed in as wide a context as possible for this class of vehicle. The guiding mission statement for this effort is in two parts:

- Investigate sensors and algorithms scalable to different vehicle sizes that compute control power margins for DEP VTOL aircraft accounting for the disturbance field and estimating local winds and gusts in real time.
- Use empirical data from algorithm use and lessons learned to suggest industry best practices and FAA policy for ensuring DEP VTOL vehicles operate safely without exceeding control power margins. Consider small UAS as well as passenger carrying DEP VTOL vehicles.

This effort examined approaches for assessing RCP and disturbance response that required increasing levels of information on the vehicle flight control system, guidance commands, and in-flight responses. Several were demonstrated in limited degree-of-freedom simulations and were initially flight tested using a modified commercially available quadcopter. The first tests demonstrated the capability of the simplified algorithm to indicate potential LOC events through monitoring command inputs to flight control actuators. Subsequent research expanded both algorithm development and data processing of both simulation and flight data to include vehicles with redundant control effectors and operations from vertical takeoff and landing to cruising flight. Based on these results, the algorithms show their utility in indicating both onset conditions of loss of control in-flight (LOC-I) due to diminished RCP and the magnitude of local aerodynamic disturbance excitation of the DEP vehicle.

1 Introduction

A major push in the development of urban air mobility (UAM) aircraft is underway that will potentially transform how we travel by providing on-demand, passenger-carrying operations in metropolitan areas. Dozens of organizations are currently in the process of developing air-vehicle concepts based on multi-prop aircraft using DEP for potential use in future air-taxi services. New standards or combinations of existing ones may be necessary to certify airworthiness and safe design of these aircraft for their use in civil service. Developing a pathway to certification requires an in-depth understanding of the flight dynamics and control characteristics of complex, multi-prop, multicomponent aircraft flying new mission profiles in urban environments.

Recent modifications in Part 23 certification requirements were implemented to change them from a prescriptive format to one that is performance based. This change allows for rapid incorporation of advanced technologies onto flight vehicles that can promote safety. This may not conveniently fit within the prescriptive certification basis structure as it exists. This research is designed to identify techniques, algorithms, and methodologies that can provide onboard Electric Vertical Take Off and Landing (eVTOL)/DEP safety assessment in real-time, supporting this transition to performance-based certification standards.

LOC-I events stubbornly remain the leading cause of general aviation (GA) aircraft accidents. This issue for eVTOL/DEP aircraft must be mitigated as they enter the transportation system Like conventional helicopters, eVTOL/DEP aircraft will exhibit some form of open-loop instability, particularly at hover, requiring feedback to the onboard control system or pilot for stabilization. While modern flight controls can provide good response characteristics to the pilot, it is important to realize that, for open-loop unstable systems, those feedbacks only marginally stabilize the underlying vehicle dynamics. That is, if the controls become inoperative or saturated (at their limit positions), the vehicle reverts to its open-loop condition which could easily lead to a LOC-I event. Having an on-board capability to actively monitor a flight vehicle's remaining control power would give a direct indication of an approach to this potential LOC-I event, guiding some appropriate action to mitigate the cause for that condition.

While knowledge of current control inputs relative to their limiting values is of great interest to a specific aircraft configuration and operating state, it is not sharable information that is easily interpreted by other DEP aircraft operating in the vicinity of that vehicle. The need for additional control inputs on the vehicle arises from disturbance suppression objectives. It would also be useful for the statistics associated with that disturbance to be estimated/measured and

communicated to other aircraft in the immediate area of operations. Such information transfer is like current pilot reporting (PIREP) of environmental conditions to air traffic control (ATC) centers. Having such information available could provide hazard warnings to other aircraft or promote operational changes in approach and departure paths around a vertiport receiving eVTOL/DEP aircraft. A parallel effort for algorithm development able to extract information on environmental conditions, based on vehicle response models, is included as part of this effort.

This research program conducted comprehensive modeling and analysis to achieve the following objectives:

1. Evaluation of approaches for real time control power margin and wind monitoring including determining vehicle control states to monitor and the impact of vehicle size, configuration, and degraded mode (e.g., thruster out) conditions.
2. Identify the most promising approaches and assess them within a representative vehicle using simulation modeling capability.
3. Demonstrate the concept in batch and real-time manned simulator trials, and in flight tests using a sub-scale Unmanned Aircraft Vehicle (UAV).
4. Evaluate implications for eVTOL and Unmanned Aircraft System (UAS) certification requirements.

2 Remaining control power estimation

Air vehicle controllability is fundamental to both safety and utility, as the aircraft controls must be capable of:

- trimming the vehicle in all phases of flight,
- providing added forces and moment for maneuvers, and
- compensating for disturbances encountered throughout the flight profile.

Unstable aircraft are stabilized, through automatic or manual control, if the vehicle's controllability is of sufficient power and responsiveness to provide appropriate forces and moments to maintain flight operations. Much like conventional helicopters, eVTOL/DEP vehicles are intrinsically unstable in hover and require such control for rotor-borne flight operations. Feedback control for stabilization subtracts from the control power available for maneuvering and trim. However, these same aircraft, due to their placement of many motor-driven force generators around their vehicle exterior, often have redundant control capability

(also called over-actuated aircraft). This can provide additional options for changes in flight vehicle states for executing certain maneuvers (e.g., separation of vehicle pitch attitude and velocity regulation, (Stoll, 2022). These additional controls may also be leveraged to maintain trimmed flight in failure states' However, this may result in potentially reduced vehicle acceleration or maneuvering options. A useful metric for assessing RCP on eVTOL/DEP aircraft must account for these impacts on the control system if it is to serve as an indicator of potential for LOC events.

Recent work (List & Hansman, 2019) directly addresses the use of control power ratios as metrics of vehicle controllability for multicopter eVTOL concepts. While this work generated ratios using torque measurements on lift rotors, other control metrics may be needed for other configurations and flight modes. Fundamental to the use of remaining control power as a metric of potential for safety monitoring is the assumption that situations leading to control saturation constitute LOC events. While such a characterization is generally true, there exist situations when maximum performance is requested from a flight vehicle, and where some controls may be at their limit values (e.g., throttle settings on takeoff). In addition, these limits on remaining control power can exist at several places within the control system itself. For pilot-controlled vehicles, stick/effector gearings may drive what vehicle control settings are possible, while physical installations of actuators and connected vehicle mechanics may have limits of their own on both displacements and actuation rates. Even the on-board control law may include limits of outputs to actuators mitigating cases of potential hard-over commands or undesired runaway behavior, especially in limited-authority feedback systems. The approach of vehicle/system control limits alone are not representative of safety margins. Instead, it is the sum of the current control power, and remaining control power required to compensate for vehicle response, other than that commanded by the current control inputs, which is of interest. Figure 1 shows a conceptual picture of the contributions of ratioed trim inputs, maneuver commands, and disturbance rejection inputs on remaining available control power (shown shaded in green).

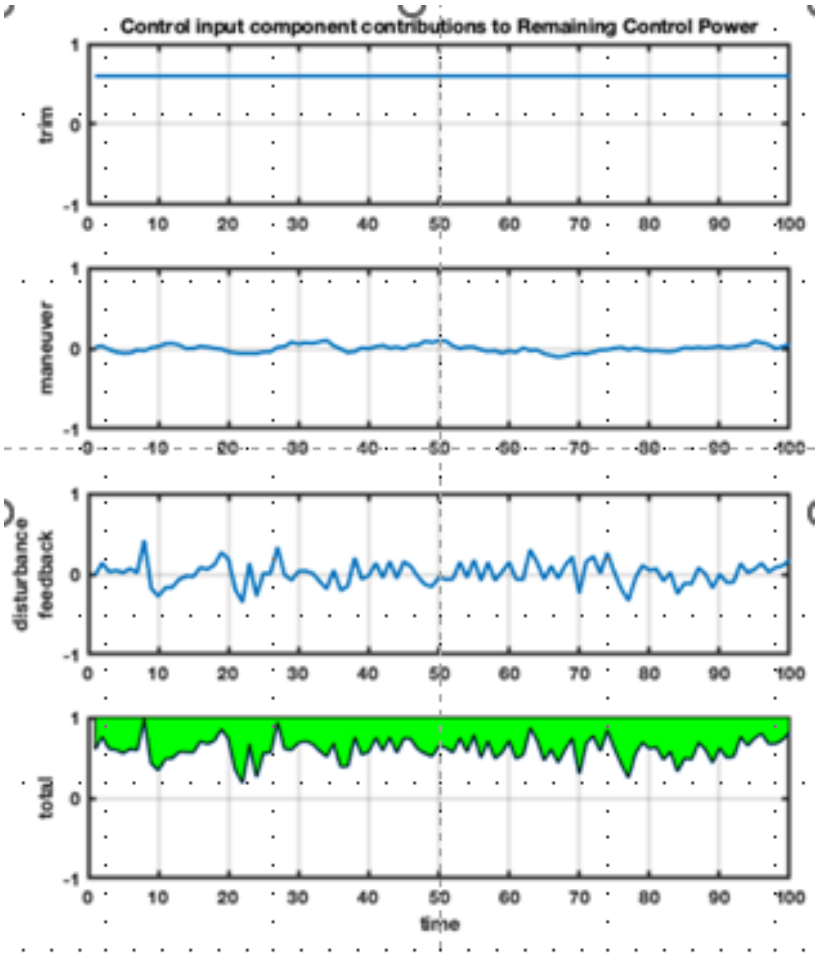

Figure 1. Contributions of control input sources to RCP

2.1 Control power metrics

Monitoring of all signals within the flight control system for possible limits exceeded that provide protection from LOC events is impractical, particularly for any system of even moderate complexity. The choice of control input that directly impacts the associated force/moment generator on the aircraft is most appropriate when a monitoring system is as generic as possible across the range of eVTOL/DEP aircraft. For rotors/propellers, this represents any control features available for changing thrust magnitude or direction. Control deflections of devices that change local camber, or sectional shape suffices for fixed-wing surfaces.

Past monitoring of pilot effector displacements relative to physical limits has been effective for assessing potential LOC situations in flight test campaigns, The redundant control configurations found on proposed eVTOL/DEP aircraft, and the potential for fully autonomous (unpiloted) operation make this alternative more beneficial. An example of an autonomous octocopter having four displaced coaxial rotors, and no pilot effectors serves to illustrate this scheme.

Monitoring of each rotor's input command (rpm or collective) provides indication of its operating state and potential for thrust/torque magnitude changes. This does not require measurement availability of guidance and control commands from the autopilot directing the vehicle's flight profile between takeoff and landing destinations. In the event of a single motor failure and subsequent additional thrust generated from the companion unit on that coaxial rotor installation, the new command for the "working" rotor directly indicates its operation at a state nearer maximum capability (reduced control power margin). It generates approximately twice the thrust previously applied prior to the fault condition. Due to the fault accommodation of the feedback control system, this change is not reflected in monitoring of the internal flight command signals within the navigation autopilot.

eVTOL/DEP aircraft designs directly capitalize on the recent developments that significantly boosted the power/weight ratios of electric motor drives, permitting their use in aviation applications. By distributing the sources of lift and propulsion, each rotor/propeller is made smaller as it is not necessary to carry the full vehicle weight or drag load on its disk. By exploiting the convenience of individual electronic control, weight savings is realized through the elimination of mechanical cross-shafting between propulsors and lift systems. This electronic control can also use direct motor speed control as a means of power/torque regulation at each rotor/propeller, potentially eliminating requirements for variable pitch control (collective and cyclic). However, this choice of control variable has some consequences.

Direct RPM or motor torque control, in the absence of rotor/propeller pitch adjustment, requires the blades to be accelerated or decelerated to the operating RPM needed for the desired level of thrust generation. The size of the rotor dictates the associated inertia and the resultant time constant for that RPM change. This controls the available bandwidth in force modulation for that type of control (Withrow-Maser, Malpica, & Nagami, 2020). Conversely, direct pitch adjustment can provide an accelerating effect on force control. Direct thrust change is first realized prior to the rotor/propeller wake adjusting to the new pitch change, mitigating some of the initial effect from that perturbation in control.

Ratioing the current control input to a "prime mover" (force/moment generator) on a flight vehicle to its input range gives a fraction of control expenditure. Subtracting that value from its limits gives a resulting ratio of remaining control power or authority for that input. An easily computed metric for RCP on input *i* is:

$$RCP_i = min\left(2\frac{u_{max}-u_i}{u_{max}-u_{min}}, 2\frac{u_i-u_{min}}{u_{max}-u_{min}}\right) \quad 1$$

This metric generates a value of 1 when the control input is at the center of its range of travel, and 0 when it reaches an upper or lower control limit bound. This value has the distinct advantage that *only the control limits available on the prime mover are necessary for its computation*, as it is agnostic of vehicle type, configuration, or operating state. While those are desirable features, use of this metric for safety assessment assumes that the aircraft is in controlled flight if this value is below unity, and this metric only has safety assessment value to the aircraft on which it is being computed. If considerations of vehicle response to this control are included in the safety assessment, via a different metric for remaining control power, or if any predictive capability is desired to assess needs for added control power, a model-based algorithm of some order must be used.

2.2 Model-based metrics

Monitoring control activity in real-time during flight operations using a model-based algorithm can have an additional benefit of providing estimates of disturbance effects. Responses not due to control application occur solely from external flow fields assuming controls on all force generators are nominal. Several researchers have developed algorithms for estimation of "wind states" that generate vehicle disturbances from comparisons between calibrated vehicle responses to control inputs and actual measured vehicle sensor data (McConville, Richardson, & Moradi, 2022; McKillip R. , 2018). Such estimates could potentially indicate turbulent environments within the current operational area that make continued flight too risky. Or they may require revision such as approach/departure directions, vehicle headings on takeoff and landing, etc. Turbulent environment information could also be *shared among other nearby aircraft*, providing enhanced situational awareness and safety, as wake turbulence warnings are often issued for local airport operations currently.

The relationship between control power and disturbance effects was investigated by researchers at NASA Ames (Lusardi, Blanken, & Tischler, 2003) in the development of the concept of mixer equivalent turbulence simulation (METS), or control equivalence turbulence input (CETI). This technique computes the residual between measured helicopter response and predictions from measured control inputs. It is processed through an inverse dynamic representation of the flight vehicle to estimate the *equivalent amount of additional control needed to generate that differential* (Seher-Weiss & von Gruenhagen, 2009). The primary use of this representation was to permit simulation of turbulent effects in manned simulation trials. If the combined or summed current control input levels, and the negated additional control that creates the disturbance, approach the limits on control capabilities of the flight vehicle, the potential for upset and loss of control is greatly increased. Although this represents a direct relationship between disturbances

present and the required control to counter them, it requires use of an inverse dynamic model and is less vehicle-uncertain in its application versus the simpler input-oriented technique described above.

Both approaches for determining either atmospheric disturbance effects on vehicle response, or equivalent disturbing control inputs accounting for differences between commanded and actual vehicle response, require a mathematical model of vehicle input-output dynamics behavior. In the first case, the vehicle model must include inputs from both actuators and external winds, while the second model only requires control actuation input effectiveness models.

2.3 Algorithm classification

Three different but related algorithms were assessed in this study, characterized by both their outputs and their data sources. RCP estimation algorithms are classified as input-oriented or output-oriented:

1. *RCP input-oriented algorithms* compute actuation limitation ratios at the force/moment generators on the vehicle using only current control input values. This computation only needs current actuator input readings and knowledge of the limit positions on that actuator.

2. *RCP output-oriented algorithms* map vehicle responses due to disturbances to an estimated equivalent control perturbation, using a vehicle dynamic model. The actuation limitation ratios from above are recomputed using the current control input minus this equivalent control perturbation estimate. The result determines LOC potential if the current control and disturbance mitigating control exceed actuation limits.

The third algorithm directly estimates the disturbance environment to generate turbulence/gust statistics for sharing with other aircraft:

3. *Model-based gust algorithms* map the vehicle response due to disturbances to a vehicle-centric model of gust sensitivity, estimating the gust inputs in real time using that dynamic model of response.

It is important to recognize that all three algorithms require information on the vehicle actuation capabilities. The model-based approaches include additional requirements for dynamic response to those actuator inputs (RCP), and for the direct gust estimation, the dynamic response to atmospheric disturbances. None of them need detailed information on the design, structure, or implementation of the on-board flight control system, as the approaches are vehicle-centric and not complete system-centric. This approach is in keeping with the fundamental definition of

control power as the capability of the aircraft to generate trim forces and moments, provide maneuver commands or accelerations, and mitigate disturbances through aerodynamic means. Some details on these algorithms are given in the sections that follow.

3 Dual-estimator approach

The model-based approach adopted in the research is effectively two-fold but has origins in the same basic concept. The vehicle is treated holistically such that total vehicle response is either due to applied control from on-board effectors, or from external disturbances. This same concept was used at Continuum Dynamics, Inc., CDI, most notably for icing accretion estimation based on measured performance metrics on an aircraft (McKillip, Keller, & Kaufman, 2002). The same estimator-based approach here is tasked with providing two metrics: the additional required control power to counter the disturbance measured on the flight vehicle, and the magnitude and type of the external disturbance. The first of these is of direct interest for maintaining adequate control of the vehicle on its intended flight trajectory, while the second is of general interest to other aircraft operating in the vicinity of the present DEP vehicle computing that disturbance estimate. The remaining control power available directly impacts the present vehicle's level of safety, while the external gust disturbance estimate provides vehicle context-free information for sharing with other aircraft of different sizes and configuration. This compares to meteorological aerodrome reports (METAR) and pilot report (PIREP) information that is provided to pilots.

3.1 Control equivalent turbulence estimation

Generation of equivalent control power for mitigating a disturbance is effectively accomplished with the METS/CETI schemes, although here it is implemented in a real-time, time-domain context. A simple example looking at linearized (stability derivative) pitch-plane dynamics of an aircraft provides an example. When considering the linearized response to both control input, primarily a moment command, and a longitudinal gust as:

$$\frac{d}{dt}\begin{Bmatrix} u \\ q \\ \theta \end{Bmatrix} = \begin{bmatrix} X_u & X_q & -g \\ M_u & M_q & 0 \\ 0 & 1 & 0 \end{bmatrix} \begin{Bmatrix} u \\ q \\ \theta \end{Bmatrix} + \begin{bmatrix} 0 \\ M_\delta \\ 0 \end{bmatrix} \{\delta_{lon}\} + \begin{bmatrix} X_u \\ M_u \\ 0 \end{bmatrix} \{u_{gust}\} \quad (2)$$

We can introduce an equivalent CETI gust "control" input in this same axis:

$$\frac{d}{dt}\begin{Bmatrix} u \\ q \\ \theta \end{Bmatrix} = \begin{bmatrix} X_u & X_q & -g \\ M_u & M_q & 0 \\ 0 & 1 & 0 \end{bmatrix} \begin{Bmatrix} u \\ q \\ \theta \end{Bmatrix} + \begin{bmatrix} 0 \\ M_\delta \\ 0 \end{bmatrix} \{\delta_{lon}\} + \begin{bmatrix} 0 \\ M_\delta \\ 0 \end{bmatrix} \{\delta_{gust}\} \quad 3$$

and augment the state variables to treat this equivalent gust control as a random process:

$$\frac{d}{dt}\begin{Bmatrix} u \\ q \\ \theta \\ \delta_{gust} \end{Bmatrix} = \begin{bmatrix} X_u & X_q & -g & 0 \\ M_u & M_q & 0 & M_\delta \\ 0 & 1 & 0 & 0 \\ 0 & 0 & 0 & 0 \end{bmatrix} \begin{Bmatrix} u \\ q \\ \theta \\ \delta_{gust} \end{Bmatrix} + \begin{bmatrix} 0 \\ M_\delta \\ 0 \\ 0 \end{bmatrix} \{\delta_{lon}\} + \begin{bmatrix} 0 \\ 0 \\ 0 \\ 1 \end{bmatrix} \{w_g\} \quad 4$$

This formulation is used in a recursive estimator, such as a Kalman filter, to determine the unknown equivalent gust control input, and its variance or statistics, in real-time, on an aircraft. It only requires a reasonable linearized dynamic model of its response. This time-domain formulation has several advantages:

1. Direct representation of gust-equivalent controls within the dynamics equations avoids a requirement for conversion to frequency-domain parameterizations and inverting multiple transfer function expressions.
2. Gust control effects excite all dynamic modes that are affected by the available control components and can include all cross-couplings and interactions that may be present on a particular vehicle configuration.
3. Time-domain representation allows for tracking transient behavior and avoids inherent lags associated with representing signals in the frequency domain.
4. Model adjustment of control effectiveness is applied for cases of reduced or inoperative control capability, with the gust control estimates adapting accordingly based on the updated dynamic model.
5. Steady-state filter estimator variance are used to optimize the selection of vehicle sensors (resolution, noise floor, sampling rate, etc.) for determination of this equivalent control gust value.
6. On-line estimation of gust control variance provides added support in the determination of control limits that warrant remedial action or termination of flight activity.

7. Choice of control for force/moment generation (individual components) or response command (vehicle force/moment aligned with an axis) are accommodated in this simple model formulation.

This approach effectively maps the actual dynamic system response to a gust, to the system response to a control input, and gives an estimate of the *equivalent control that must be supplied to counter the disturbance of the gust on the aircraft*. A simple model for a quadcopter demonstrates that this technique provides a reasonable assessment of the equivalent control needed for generating a similar disturbance, as shown in Figure 2. This plot shows the actual response of the simulation model to a random gust calculated from using the estimated equivalent control gust input to generate a control response. Apart from some high frequency tracking error, the estimated control gust magnitude provides a good estimate of how the vehicle responds to turbulence. This is an appropriate metric to determine what ideal control is needed to counter those effects. With this computed equivalent disturbance "control," the previous RCP metric is modified to use:

$$u_i = \delta_{control} - \delta_{gust} \tag{5}$$

This implies that if the disturbance effect cannot be accommodated with the current control and the ideal disturbance correction input, a control limit may occur resulting in a potential LOC event, provoked by an excessive disturbance on the aircraft. Note that prediction of this control limit is not dependent upon any knowledge or assumptions concerning on-board feedback control functions, but on a reduced-order model of the open-loop vehicle dynamics. An alternative use of the estimated equivalent disturbance control from the filtering process could include adding its estimation variance to this sum providing even more margin of protection from this stochastic (random variable) disturbance input.

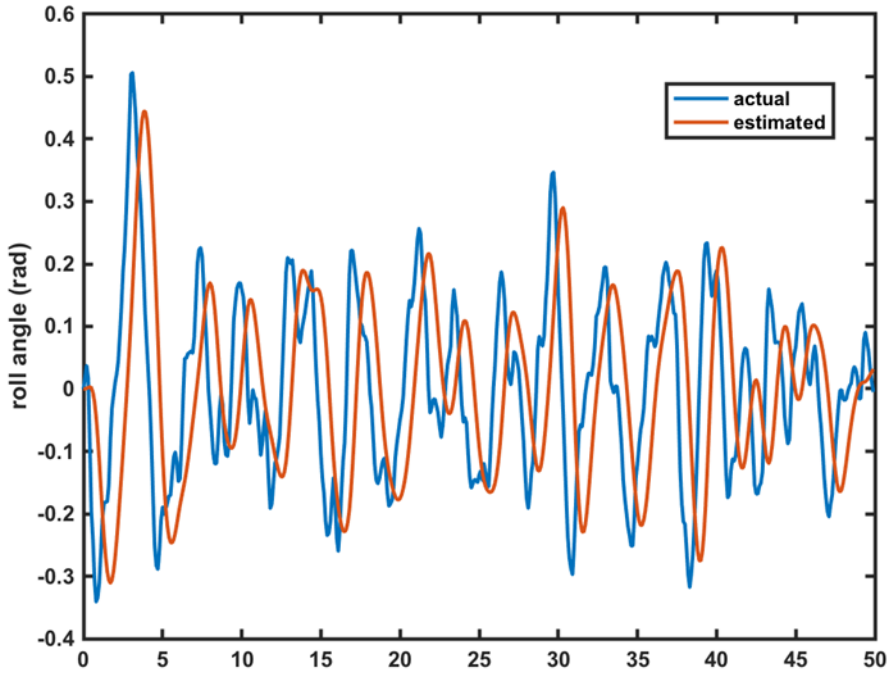

Figure 2. Simulated quadcopter response to gust and to control equivalent gust input

3.2 Recursive gust estimation

Knowledge of vehicle control activity relative to its limitations is a viable indicator of the potential for a LOC event. However, the ability to directly sense or estimate the current environmental disturbance can provide an additional safety buffer on the amount of control power required to maintain adequate flight control and operational safety. Such information may be represented in the vehicle operator's manual or may be used in flight dispatch functions for enforcing limits on acceptable landing and departure operations.

Sensing of the turbulence environment using on-board systems is done using discrete sensors or a holistic, performance-based method. The models for full vehicle responses to turbulence are used to estimate what aerodynamic environment generated that response. In some sense, these two approaches are equivalent, except the holistic aircraft response approach requires the inversion of a higher-order dynamic model. Direct turbulence sensors include air data probes of appropriate bandwidth, autorotating propellers, or flow-angle vanes. Indirect vehicle measurements that show evidence of disturbances range from isolated accelerometers to full inertial measurement units (IMUs) with possible GPS-aided position and velocity data for a complete vehicle state estimation application. This can include gust disturbance states. Each approach has its benefits and disadvantages.

Discrete sensors typically represent a simpler approach for detection of flow states on an aircraft but must be placed in locations that do not have undue influence from local flow effects. These arise from changes in secondary flows from operating state adjustments or interacting wake/wash effects. This interaction is why most flight test aircraft operate with long booms positioned forward of aircraft structure to sample flow conditions ahead of vehicle upwash and other flow gradients. A disadvantage of discrete sensor application is the requirement for extra hardware, power, and data transfer.

Similarly, complete holistic vehicle sensing must include all relevant effects in the system model if it is to unambiguously identify flow state changes from external disturbances, versus those from local trim changes or dynamic maneuvers. This separation is achieved through monitoring vehicle control commands and processing them with a dynamic model of the vehicle, generating an estimate of expected controlled response, and determining the measurement residual due to external disturbances. Although this approach needs good measurement of control inputs, vehicle response, and a valid dynamic model, it does not carry an additional size, weight, and power (SWaP) requirement, as the sensing is performed algorithmically.

Direct turbulence field estimation is viewed as a more global assessment of the vehicle disturbance environment than the control equivalent turbulence estimation approach. While knowledge of the control equivalent turbulence input to a specific aircraft is useful for assessment of potential loss of control from exceeding control power requirements on that vehicle, it is not generally transferrable information that has value to other disparate aircraft that may be operating in the same area. Direct estimation of gust velocities, however, are generally shared among aircraft operating near one another (e.g., METAR reports on gusts), but still require aircraft-specific interpretation to gauge the severity of that measured disturbance.

Consider a simplified linearized model for longitudinal response and note that most of the significant impact of gusts on vehicle ride quality affects the short period response. This limits the states of interest to include vertical velocity, pitch rate/pitch attitude, and vertical gusts, resulting in the following dynamic system which models the vertical gust as a first-order random process driven by white noise:

$$\begin{bmatrix} \Delta\dot{w} \\ \Delta\dot{q} \\ \Delta\dot{\theta} \\ \Delta\dot{w}_g \end{bmatrix} = \begin{bmatrix} Z_w & u_0 & -g\sin\theta_0 & -Z_w \\ M_w + M_{\dot{w}}Z_w & M_q + M_{\dot{w}}u_0 & 0 & -M_{\dot{w}} - M_{\dot{w}}Z_w \\ 0 & 1 & 0 & 0 \\ 0 & 0 & 0 & -1/\tau \end{bmatrix} \begin{bmatrix} \Delta w \\ \Delta q \\ \Delta\theta \\ \Delta w_g \end{bmatrix} + \begin{bmatrix} Z_{\delta e} & Z_{\delta T} \\ M_{\delta e} + M_{\dot{w}}Z_{\delta e} & M_{\delta T} + M_{\dot{w}}Z_{\delta T} \\ 0 & 0 \\ 0 & 0 \end{bmatrix} \begin{bmatrix} \Delta\delta e \\ \Delta\delta T \end{bmatrix} + \begin{bmatrix} 0 \\ 0 \\ 0 \\ 1/\tau \end{bmatrix} [v2] \quad (6)$$

This representation lends itself directly to implementation of a Kalman filter for estimating aircraft states along with noise values that include variance estimates as part of the covariance calculation within the filter structure. The approach has several advantages which include:

1. Direct estimation of gust disturbance in real-time using aircraft instrumentation.
2. Simplified algorithmic processing that is low-order and easily hosted on available processors.
3. Computation of gust metrics that are not vehicle-specific and are shared with nearby aircraft for their own safety assessment.

This representation, however, may not always capture the primary gust effects encountered by an eVTOL/DEP configuration, particularly if spatial distributions of the gust (gust gradients) are on the same length scale as the distances separating lift rotors. In those events, significant moment inputs are expected on the vehicle other than those from a "uniform" gust value distributed across the airframe. It may be of interest to include equivalent pitch rate "gust" effects for this restricted longitudinal model as well, expanding the degrees of freedom that would be used to represent the turbulent environment surrounding the aircraft.

3.3 Estimator structure and implementation

Both model-based RCP and gust estimation approaches use a recursive Kalman filter estimate that incorporates a locally linearized dynamic model (often called a stability derivative model) of the aircraft response. Kalman filters provide tracking performance of the estimation process using feedback of the error between the measured system response and that predicted by the process model. The design of the filter optimizes the feedback gains on those errors to generate minimum variance estimates of the system states. This is based on given known or estimated Gaussian noise characteristics both disturbing the system process and corrupting the sensor measurements of the response.

A block diagram of the model-based RCP approach for estimating the control equivalent turbulence for the aircraft is shown in Figure 3, where the flight control system (FCS), w is the external gust disturbance, u is the vector of actuator inputs to the aircraft, and y is the vector of sensor measurements. All items below the red dashed line are components of the algorithm, with hatted quantities representing estimates of state vectors and rates, control equivalent disturbances and rates, and sensor output estimates. These combine with actual sensor measurements to generate an error to provide feedback tracking capability. The estimated control equivalent disturbance is subtracted from the measured actuator inputs to provide an augmented input for

use in comparison against the available actuator input limits, as done in the input-oriented algorithm. This generates a numeric RCP that includes the required actuator inputs to mitigate the disturbance effects on the aircraft.

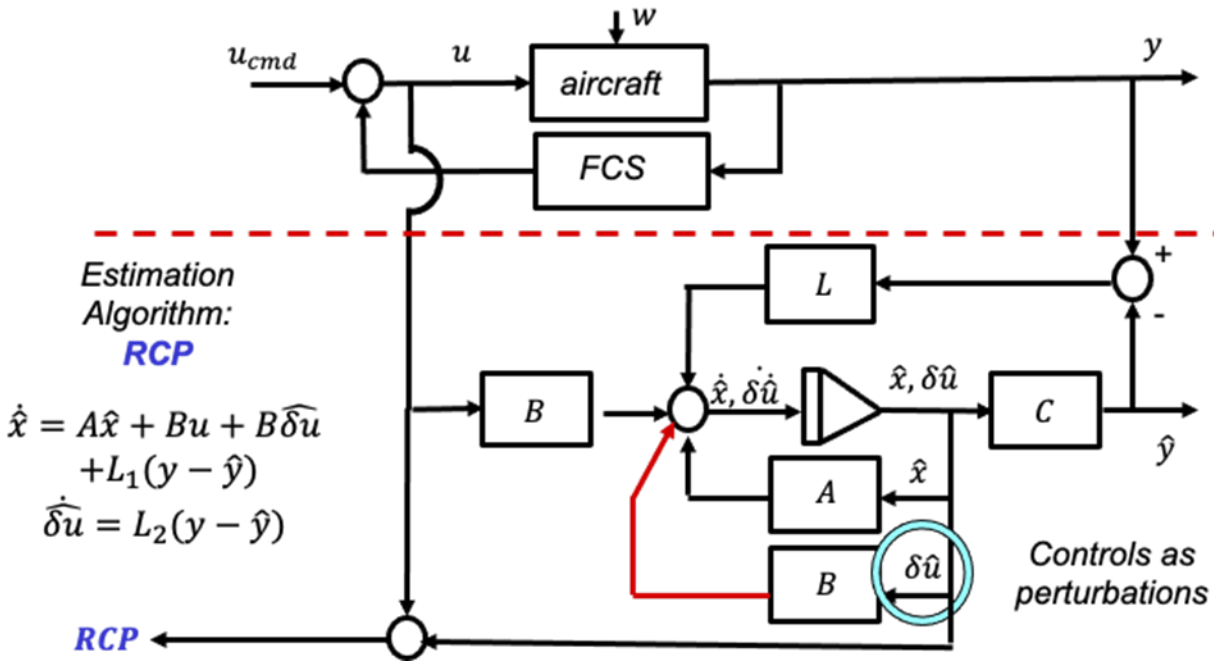

Figure 3. RCP algorithm schematic showing estimated control equivalent turbulence input

While recognition of the presence of a flight control system is shown in this schematic, its only impact on the generation of this model-based RCP value is from the measured present input to the actuators on the aircraft platform. The design of the algorithm is not dependent upon any knowledge of the control law, structure, or modes present in that component of the aircraft system.

A block diagram of the model-based approach for gust estimation is shown in Figure 4 where the estimated gust perturbation input is estimated along with the other states in the dynamic model, and output for further processing and sharing with other aircraft in the operating vicinity. The red line feeding back to the summation junction in the algorithm is like that of Figure 3 as it represents the augmented state's contribution to the estimated state rates in the Kalman filter. However, it uses a different effectiveness matrix than for the actuator input. The other predictive components in the filter that contain the piecewise linearized system dynamics matrices are identical.

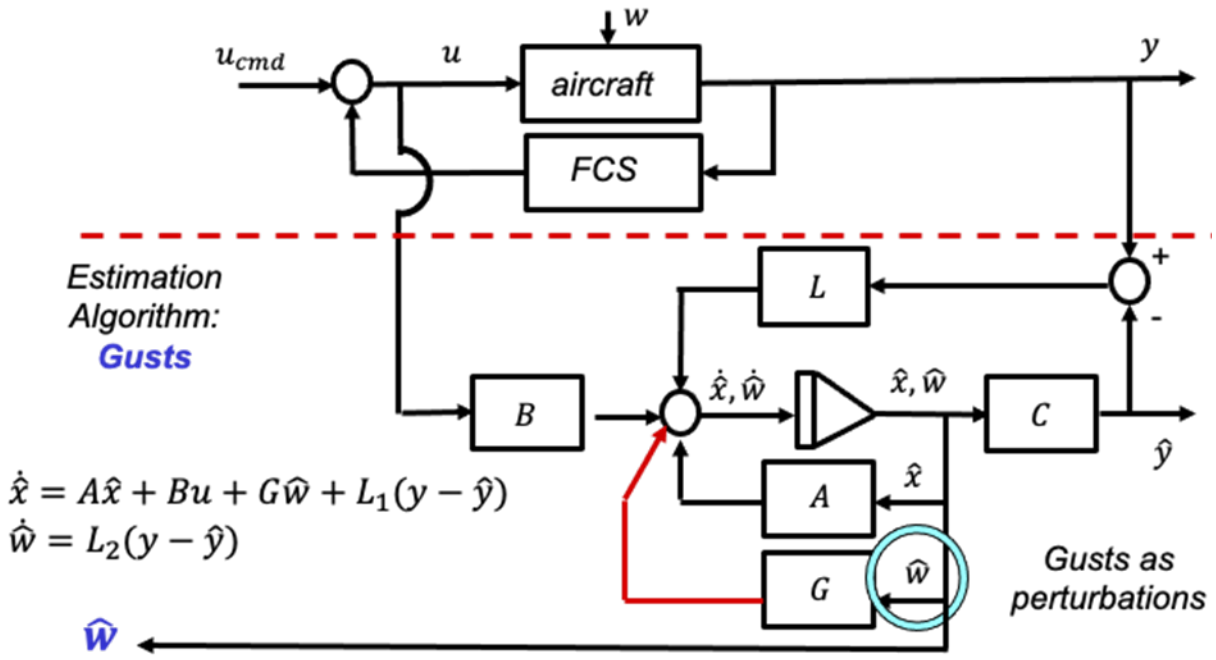

Figure 4. Model-based gust estimation schematic showing augmented gust states as outputs

The fundamental difference between these two model-based estimators is the assignment of the source of the energy, the difference between the predicted output and that measured by the aircraft sensors to either the gust states, operating through a gust effectiveness matrix G, or to the control equivalent states, operating through the control effectiveness matrix B. Having two algorithms that simultaneously process the differences between the model and actual sensor outputs operating on the same aircraft computers suggests a redundancy. A third model-based algorithm was examined that estimated the control equivalent disturbance from that state-rate perturbation generated using the estimated gust states. That state-rate perturbation could be mapped, via pseudo-inverse approximations, back to control equivalent disturbance inputs for subsequent RCP calculations. Figure 5 shows the schematic where the RCP calculation uses a pseudo-inverse of the control effectiveness matrix to compute the control equivalent disturbance for this model.

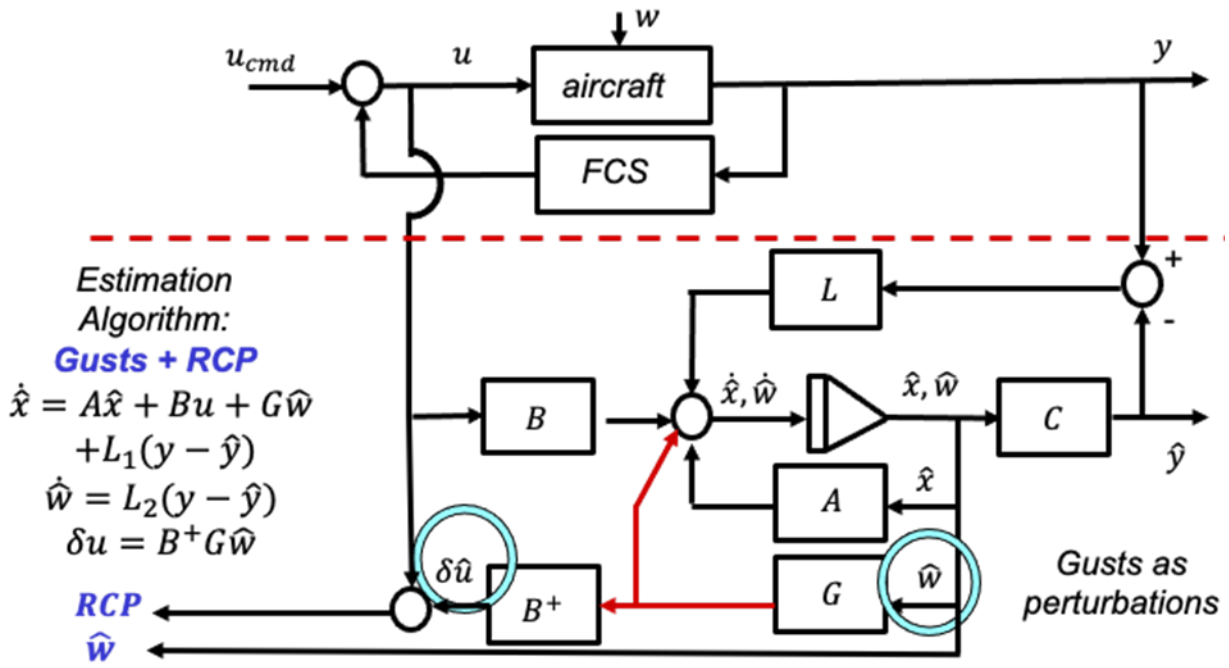

Figure 5. Combined model-based estimation of gust inputs and control equivalent disturbance

The algorithm of Figure 5 is more representative of the actual physics of the process, where the actual gust states are estimated and their effectiveness in generating state rates is used to map the control equivalent disturbance effect. However, the generation of the control equivalent input used in the resulting RCP value is dependent upon the accuracy of the gust response model for the aircraft. An alternate algorithm that helps remove this dependency, but still is implemented using a single filter structure is shown in Figure 6 where a state rate perturbation is estimated and then processed to generate both a perturbation input for use in model-based RCP estimation and direct gust perturbation inputs for data sharing with other aircraft. Both estimates use a pseudo-inverse matrix approach to map the state rate perturbations to their respective outputs, which generates a minimal norm vector estimate for each.

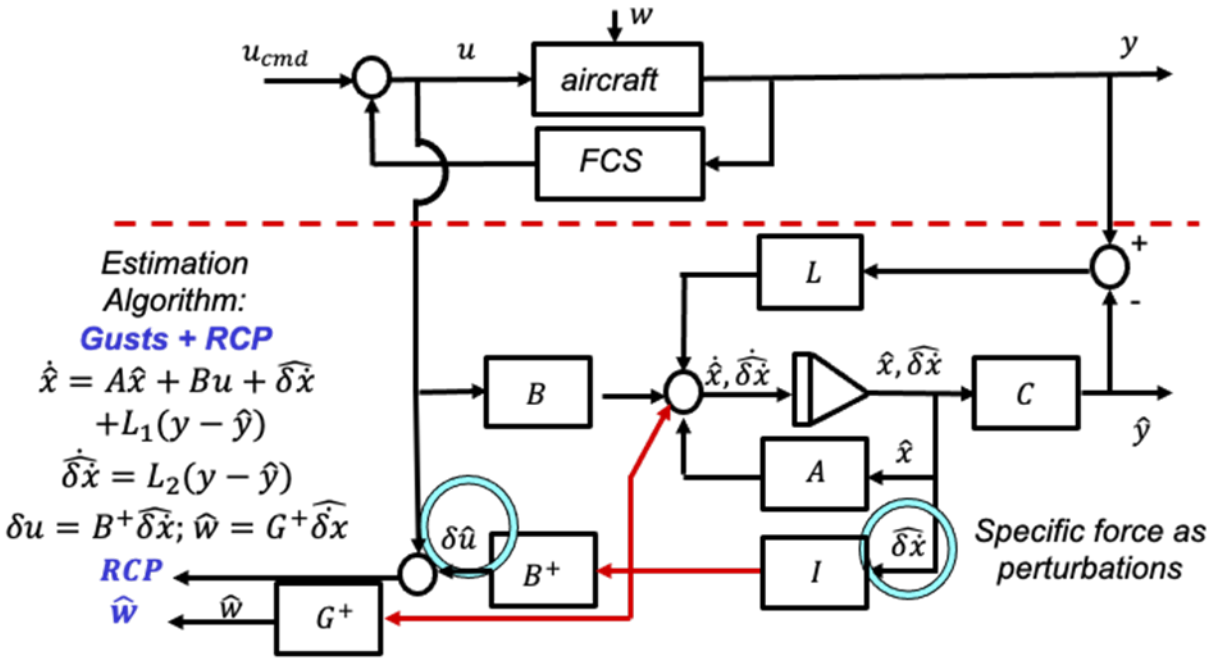

Figure 6. Combined RCP and gust estimates from estimated state rate perturbation vector

4 Simulation assessment

The limited degree-of-freedom stability derivative models have suggested this dual estimation approach is a viable technique for online estimation of both remaining control power in the presence of disturbances and the gust disturbance magnitudes themselves. However, it is not sufficient for algorithm performance testing. Also, simplified models do not capture the potentially complex interactional aerodynamic effects that gusts can have on eVTOL/DEP aircraft having closely spaced lift and propulsion rotors. More detailed models of eVTOL/DEP aircraft for several base configuration types were studied to assess their gust response sensitivity and to develop appropriate dynamic models for use within the estimation algorithm. Two sources of models were used for assessment of this dual estimation approach:

- a “stitched” locally linearized flight dynamics model produced from the NASA Design and Analysis of Rotor craft (NDARC)/Flight dynamics Computation of Ordinary Differential Equations (FlightCODE) software combination,
- and a fully nonlinear model incorporating CDI’s CHARM Module software in its CHARM Toolbox for MATLAB .NASA created representative eVTOL/DEP vehicle models using its NDARC software (Johnson, Silva, & Solis, 2018). These vehicle definitions are inputs to the recently developed FlightCODE analysis tool for the creation of locally linearized dynamic flight models of these aircraft (McKillip & Keller,

2021). FlightCODE generates extended stability derivative models of aircraft that are sized and identified within NDARC input data, representing small perturbation dynamic models at specified trim points. The linearized aerodynamic models are indexed with flight condition and vehicle configuration parameters. They are combined with trim control and body forces to couple with a nonlinear kinematic model that can create a continuous flight dynamics model using a "stitching" process, (Tobias & Tischler, 2016).

The more extensive models developed for this use incorporate features of the CHARM Toolbox for MATLAB. This incorporates the CDI CHARM Module Wake/Panel model within a MATLAB-based component formulation of an aircraft model for fully nonlinear simulation of vehicle response to both control inputs and external disturbances (McKillip, Keller, Wachspress, Whitehouse, & Quackenbush, 2010). The CHARM Module provides rapid vortex-based wake modeling for a wide assortment of flight vehicles. It is extensively correlated with wind tunnel and flight test data, and most recently is used within a fully nonlinear flight simulation tool for eVTOL/DEP aircraft called DEP aircraft Simulation (DEPSim) (Theron, Horn, & Wachspress, 2020). Locally linearized models from DEPSim were also used in the assessment of modeling level of detail needed for acceptable disturbance effect estimation.

4.1 FlightCODE models

Two flight dynamic models of the NASA single-place quadcopter, (Johnson, Silva, & Solis, 2018), were created using the FlightCODE tool for a hover condition, as takeoff and landing conditions in turbulence are likely to be defining metrics in control power requirements. The first was a simple quasi-static model with no rotor dynamics, and the second included first-order flapping along with dynamic inflow states for all four rotors. A normally distributed random vertical gust was imposed on each model to assess the difference in response between the two representations and the difficulties in use of the quasistatic model to represent gust response behavior when additional dynamics are present.

Despite the difference in stability derivatives between the two models, their gust response to the imposed random vertical turbulence is almost identical, as seen in Figure 7. This is due to the similarity in the frequency response of the two models over the low-frequency range, seen in Figure 8, where the vehicle is dominated by a heave damping response. This preliminary result suggests that, at this level of modeling fidelity, a low-order approximate model for vehicle response may be sufficient for estimating low to moderate frequency gust magnitudes This intermediate fidelity model serves a useful role in assisting in the understanding of the

appropriate level of modeling detail needed to estimate the statistics of the equivalent control required for disturbance mitigation with confidence.

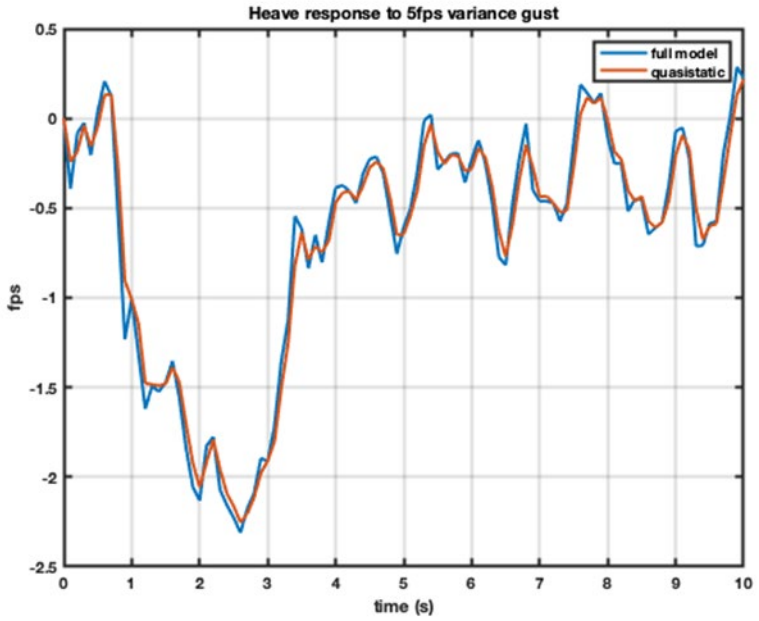

Figure 7. Heave response velocity to vertical gust for different concept quadcopter DOFs

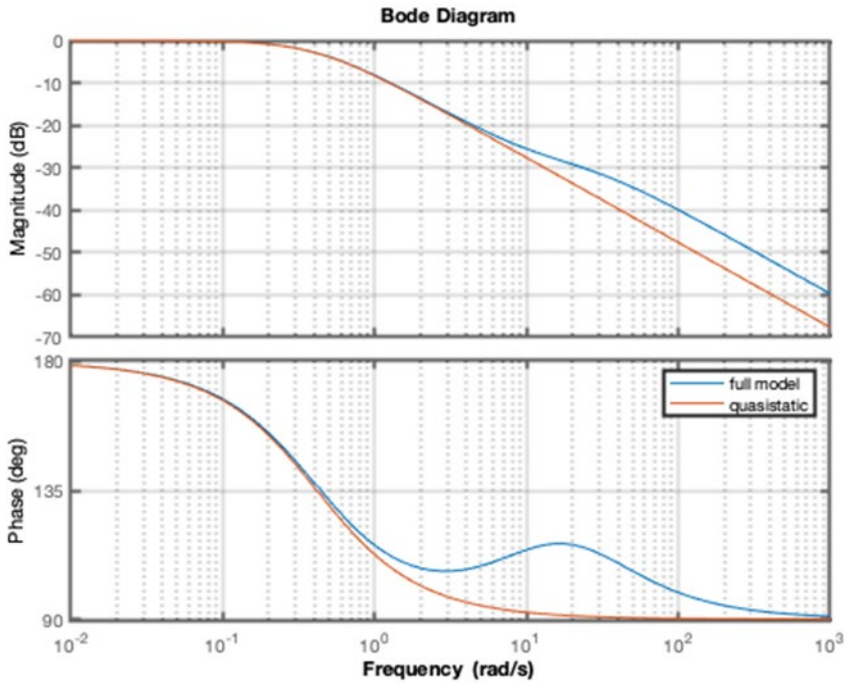

Figure 8. Quadcopter vertical gust to heave velocity frequency response, various DOFs

4.2 CHARM aerodynamic models

Parameters from the same NDARC reference model used in the FlightCODE model generation were used to create a nonlinear CHARM Toolbox model in MATLAB of the quadrotor single-place concept vehicle. This model includes a full-span wake model coupled to a blade element rotor model, currently only using rigid flap response for the blade dynamics representation. Gust modeling uses uniform variation of the local flow field, impacting local flows and wake filaments similarly, and represents a gust wavelength several times the fundamental dimension of the quadrotor vehicle. A representation of the wake structure for this aircraft in a 40kt trimmed flight condition is seen in Figure 9. The interaction of the aft rotor wakes with the forward rotor wakes is evident, despite the vertical separation of the two lift systems.

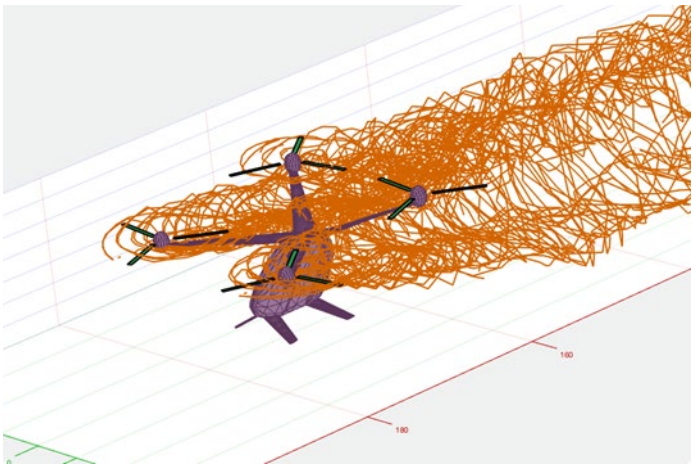

Figure 9. CHARM wake structure for NASA quadcopter at 40kts cruise

The model was extended to include mechanical time constants for supporting control designs that modulate thrust on rotor/propellers via rpm variations. Use of rpm control instead of collective pitch control requires accelerating torques to change rotor speeds. It generates a transient or dynamic effect, compounded by the change in the wake characteristics with thrust changes. To appreciate the time lags associated with wake dynamics effects, a simulation of a 10% increase in rpm for an isolated rotor shows an oscillatory transient that settles into a new steady state condition after a quarter second following the step change, Figure 10. This response does not include rotor inertia in the applied torque requirement.

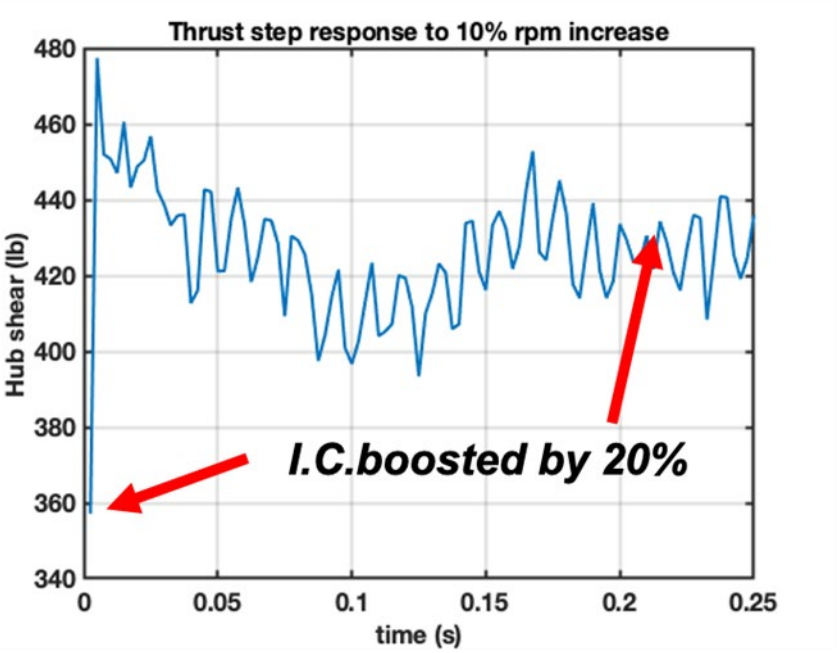

Figure 10. Hub shear transient following 10% step increase in rotor rpm

CDI and Penn State developed a simulation tool, DEPSim, that provides detailed component models of representative distributed electric propulsion aircraft. The tool includes motor dynamics, rotor dynamics with multiblade coordinates, variable rpm and full rotor collective/cyclic controls, and an aerodynamic model that uses either dynamic inflow or the CDI CHARM module for rotor and fixed-surface airload calculations. The full real-time executable form of this tool is not currently available for manned simulation evaluation of the RCP and gust estimation algorithm. The model is used to support algorithm development in two ways. First, to generate locally linearized flight dynamic models that include aircraft rigid body states and component dynamics, with trim values for those state variables and control inputs. The linear models are generated at 20 knot increments, for rpm-controlled and full cyclic-controlled rotor configurations, and hover to 140 knots for the ”generic” lift plus cruise (LpC) configuration shown in Figure 11. This aircraft represents a four-passenger eVTOL/DEP concept configuration that flies like a multicopter in hover, and transitions to wing-borne airplane-like flight in cruise (lift rotors stopped and indexed fore-aft) on the respective support booms.

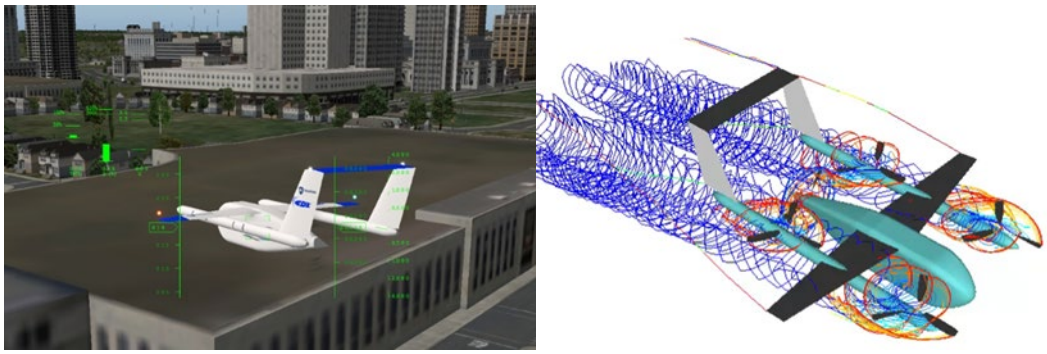

Figure 11. CDI/PSU LpC configuration in X-Plane and with a CHARM wake

The second use of the model includes response simulation to gusts that incorporates the full CHARM wake model but running off-line in a time-marching simulation. Figure 11 represents the DEPSim model in hover hold operation on the lee side of a hangar building, with a CFD-calculated turbulent air wake shed from the building edges. This represents the flight test conditions used in (Lusardi, Blanken, & Tischler, 2003) which determines CETI frequency response curves for modeling gust response for a UH-60 helicopter.

4.3 Evaluation goals

Simulation studies were designed to check the assumptions associated with the algorithms for both RCP estimation and gust estimation, which include:

- The algorithms are applicable to the broad class of eVTOL/AAM configurations that include multicopters, lift plus cruise arrangements, and vectored thrust vehicles.
- Simplified dynamics of rigid body response are applicable to handling qualities frequencies (e.g., short period dynamics) and are appropriate for both equivalent disturbance control estimation and gust estimation.
- Estimation results are sufficiently uncertain to types and configurations of flight control systems and autopilots, as the algorithms use only vehicle-centric data.
- Algorithms are adjusted for changing flight conditions and operating configurations through velocity and configuration scheduled linearized math models.

4.4 Combined gust and RCP estimation

A CHARM-based aerodynamic model for the quadcopter was simulated in hovering flight with simple stabilizing feedback while excited with a bandwidth-limited gust disturbance in all three axes. The estimation algorithm indicated in Figure 6 was applied to the vehicle response states estimating the state rate perturbations, which mapped to both an estimated gust time history and

a control equivalent gust perturbation. Each transient for the gusts, estimated gusts, and estimated control equivalent inputs are shown in Figure 12.

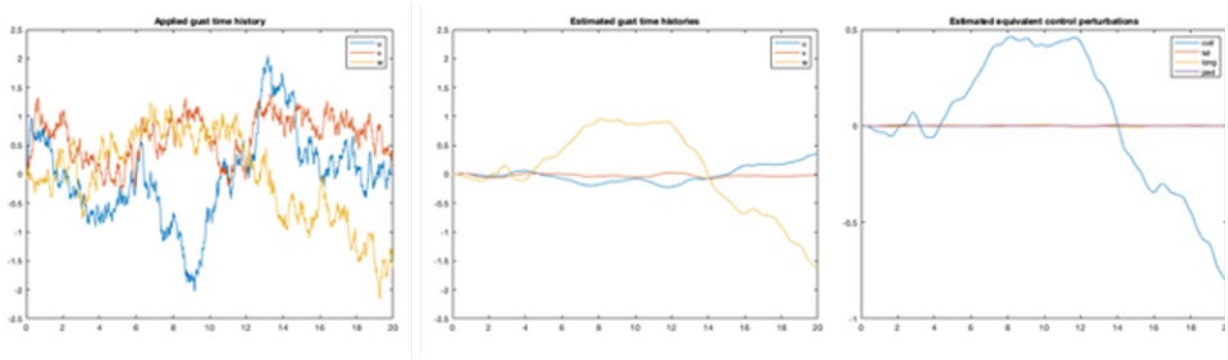

Figure 12. Quadcopter applied gusts, estimated gusts, and estimated control disturbances

Several observations are made from these estimates. The estimated gust time histories reflect a smoothed, lower-bandwidth estimate for the simulated vertical gust excitation but miss the general fluctuations of the in-plane longitudinal and lateral gust velocities. This is primarily due to the stabilized quadcopter being relatively insensitive to those gust inputs and is not an ideal sensor able to reconstruct the actual disturbance inputs. Similarly, the equivalent control disturbance estimation is dominated by an equivalent collective disturbance input, reflecting the sensitivity of the simulated quadcopter to the vertical response from the applied gust disturbance.

It is important to note that the actual RCP estimate is the combination of the current control input for each actuator and the negated equivalent control disturbance calculated here. If the control system is already compensating for the disturbance effect on the aircraft, the equivalent control disturbance generated from the algorithm is reduced in magnitude.

4.5 Model order effects on algorithm performance

Further simulation evaluations were conducted using the LpC configuration shown in Figure 11. This aircraft model uses locally linearized dynamic response models that include motor dynamics, multiblade dynamics, dynamic inflow, and rpm variations with rigid body dynamics. The range of underlying dynamic frequencies suggests a high complexity model useful to examine the algorithm performance using lower order models for the vehicle response to control inputs.

Algorithm evaluations were conducted on representations of Figure 4, Figure 5. and Figure 6, using the locally linearized LpC configuration of Figure 11. The linear model was reduced to capture the vehicle rigid body states and roll and pitch attitude states. The first three multiblade

rotor modes for all five rotors (collective and disk tilt modes), and the first three dynamic inflow modes for all five rotors. This left a 38-state dynamic model reduced from an original 62-state representation. Since the linearized model of this vehicle is open-loop unstable, a low-level stabilization feedback was designed based on feeding back the rigid body states using standard linear quadratic regulator methods. Once the model was stabilized, as determined from an eigenvalue analysis, a simulated gust was applied in the vertical axis following a raised-cosine shape, with the gust duration of 5 seconds. This was followed by no gust excitation for a remaining 5 seconds giving a 10 second response record. The raised cosine gust was used instead of a filtered random white noise excitation on all axes, to assess transient nature of the output-oriented estimation algorithms and the allocation of excitation energy within the algorithm to the estimated disturbance states (both gusts and control equivalent disturbances).

This resulted in simulation data for a high-order (38 state) dynamic model of a DEP aircraft. Included are actual gust excitation time history, aircraft state time history, and control input time history for each actuator based on the rigid body state feedback gains operating on the vehicle response time history. These data were used in all algorithm evaluations as the truth conditions compared to the algorithm estimates.

4.5.1 Output-oriented direct gust estimation

A truncated dynamic model including only the vehicle rigid body states and the roll and pitch attitudes was used to design a Kalman filter. The filter estimated an augmented form of the low-order model to include states representing gust disturbances for the aircraft (similar to the equations in Section 3.2.), but with representation for all three axes for the gust disturbance. The gusts were modeled in the filter as a random walk process, where a Gaussian white noise excites the derivative of the gust state, and the gust state itself excites the DEP vehicle model through an appropriate column of the aircraft stability derivatives. The modeling approach is standard practice to include a random variable within a Kalman filter formulation, and the bandwidth of the Kalman filter is ultimately determined by the assumed variance of the white noise source.

The results from the direct recursive filter estimate of the gust excitation is shown in Figure 13 where the raised cosine gust in the vertical axis is plotted along with the time histories of the estimated gusts. While the vertical gust estimate has a similar raised cosine character, its peak is delayed from the actual gust, and its magnitude is approximately a third of the actual excitation. Additionally, the estimated gust character shows significant energy in the longitudinal and lateral channels as well, most likely arising from the coupled response seen from the rigid body states of the aircraft.

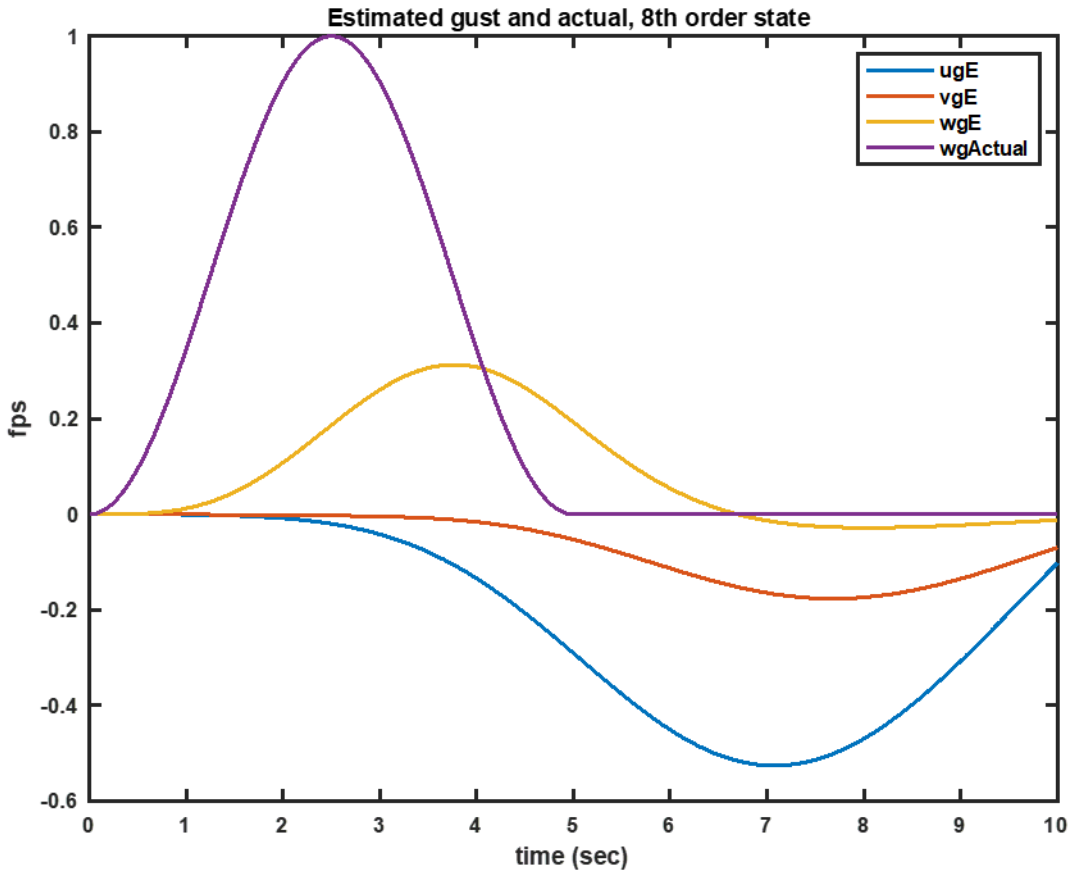

Figure 13. Actual gust and estimated gust vector for raised cosine excitation, hover conditions

A check of the tracking performance of this recursive Kalman filter operating on these simulated data are shown in Figure 14 where the actual body axes velocities from the simulation are plotted along with their estimates from the filter. Tracking performance is adequate, indicating the results of Figure 13 are to the result of the modeling features and not the adjustment of filter tracking bandwidth.

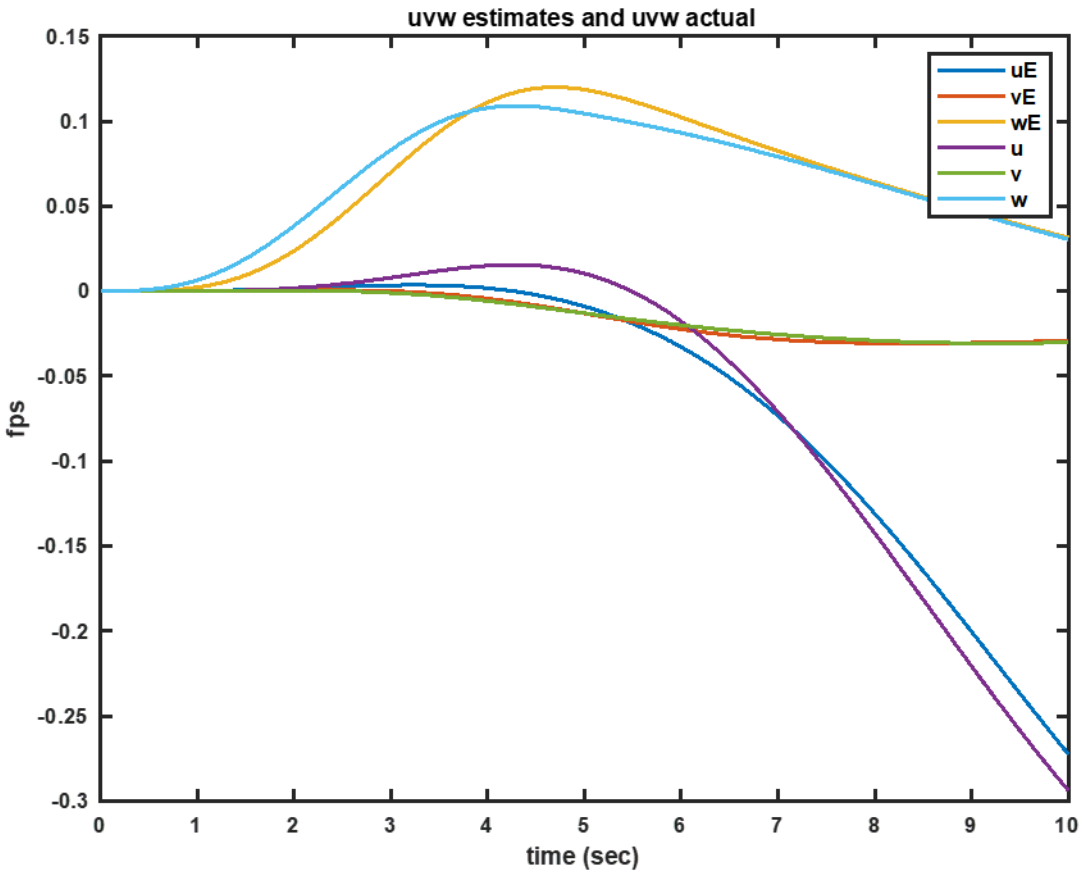

Figure 14. Raised cosine gust-excited body axis velocity responses and estimates from filter

4.5.2 Output-oriented direct control equivalent disturbance estimation

The same low-order eight-state rigid body model was used with five control equivalent disturbance states, representing the collective control on all five rotors for this configuration. The system is a model for generation of a recursive filter to estimate those disturbance states. A similar random walk model for Gaussian noise driving the disturbance states was used, and filter tracking performance was monitored through comparisons between simulated and estimated body axis velocities.(not shown). Figure 15 plots time histories of the feedback control with the control equivalent disturbance inputs. The feedback control inputs are all nominally positive in this plot, as they provide both stabilizing feedback and some disturbance suppression. The control equivalent disturbances are nominally negative, effectively generating body responses that the feedback is attempting to mitigate.

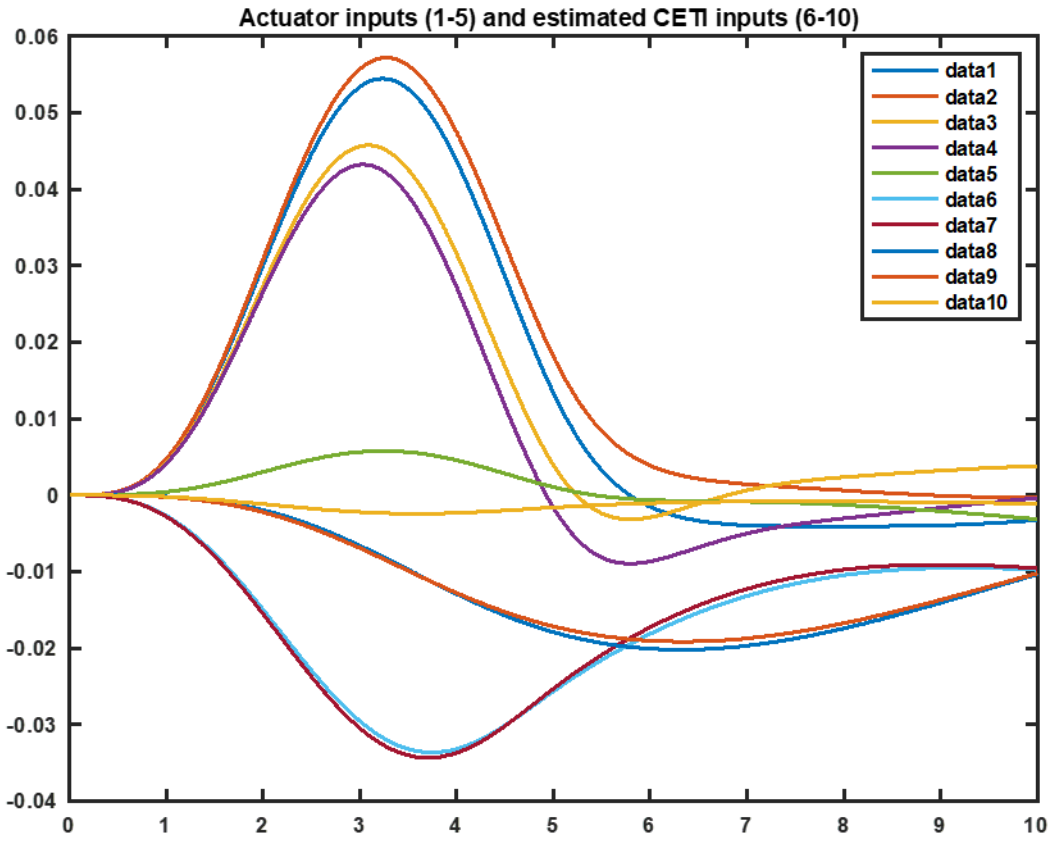

Figure 15. Simulated gust response actuator inputs/estimated control equivalent disturbances

Of interest is the relative magnitude and phasing of the control-equivalent disturbance estimates between the front rotor collectives (data6 and data7) and the rear rotor collectives (data8 and data9) for the vehicle. While the front rotor equivalent disturbance aligns with the peak feedback inputs on the front rotors in the simulation, the rear rotor equivalent disturbance indicates a peak input well past any other inputs whether feedback to the actuators or estimates of other disturbance values.

When the feedback control inputs are added to the estimated control equivalent disturbance inputs and used to drive the 38-state open-loop model of the LpC configuration, the body axis velocities generated only loosely follow those from the closed-loop LpC model, as shown in Figure 16. The discrepancy arises from two sources: the open-loop LpC model is unstable, which will magnify perturbation effects, and the control inputs do not excite the aircraft in the same way that the gust velocities do.

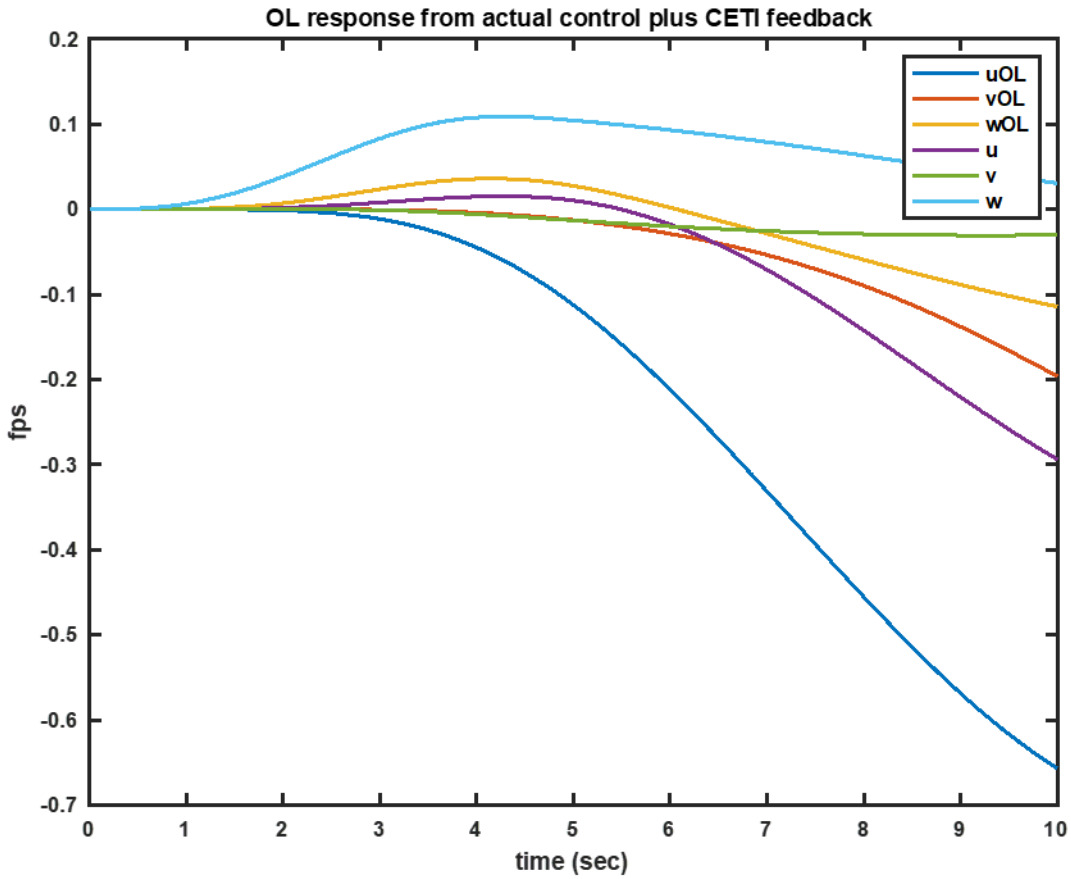

Figure 16. Open-loop body velocities from combined inputs and from simulated gust response

4.5.3 Output-oriented state rate estimation with pseudo-inverse

Finally, the estimation of state rate perturbations and subsequent pseudo-inverse mapping of those perturbations back to control equivalent inputs or gust excitation velocities was considered for low-order model assessment. Above, the 8-state model was augmented with six perturbation states representing body axis linear and rotational accelerations and was represented in the filter structure as random walk processes with white Gaussian inputs. These augmented states closely align with the differences between the model and the higher order simulation output and combine the effects of both disturbance effects and model mismatch into the perturbation estimates.

Figure 17 shows the perturbations in state rates for this model, effectively generating acceleration perturbation states for the simulated gust response. While some effect is seen for the longitudinal acceleration estimate, the responses are dominated by the vertical heave acceleration, directly driven by the raised cosine gust excitation of the simulation. Phasing of the vertical acceleration is slightly delayed from that of the actual gust velocity in Figure 13,

reflecting the finite bandwidth of the recursive filter. Estimates of body axis velocities track those from the simulation very well (not shown).

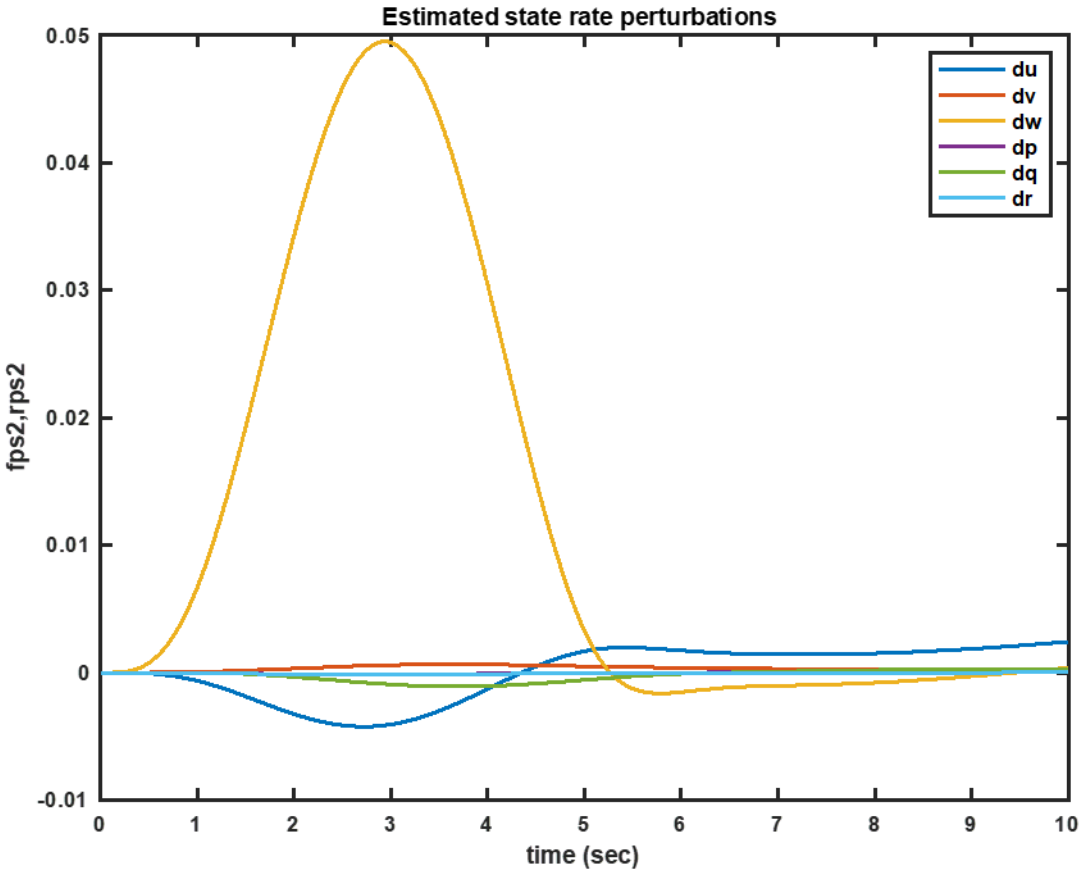

Figure 17. Estimated perturbation state rates from filtered simulated gust response

When the control effectiveness matrix and the gust effectiveness matrix are applied as pseudo-inverse operators on these accelerations, the results are shown in Figure 18 and Figure 19. Since these are algebraic operations, there is no phasing difference from the generation of the perturbation accelerations, only a recombination to reflect the levels of sensitivity of each to their respective excitations. The control equivalent inputs of Figure 18 show similarities to the feedback signals of Figure 15 and do not have the somewhat slower character from the direct filtering algorithm.

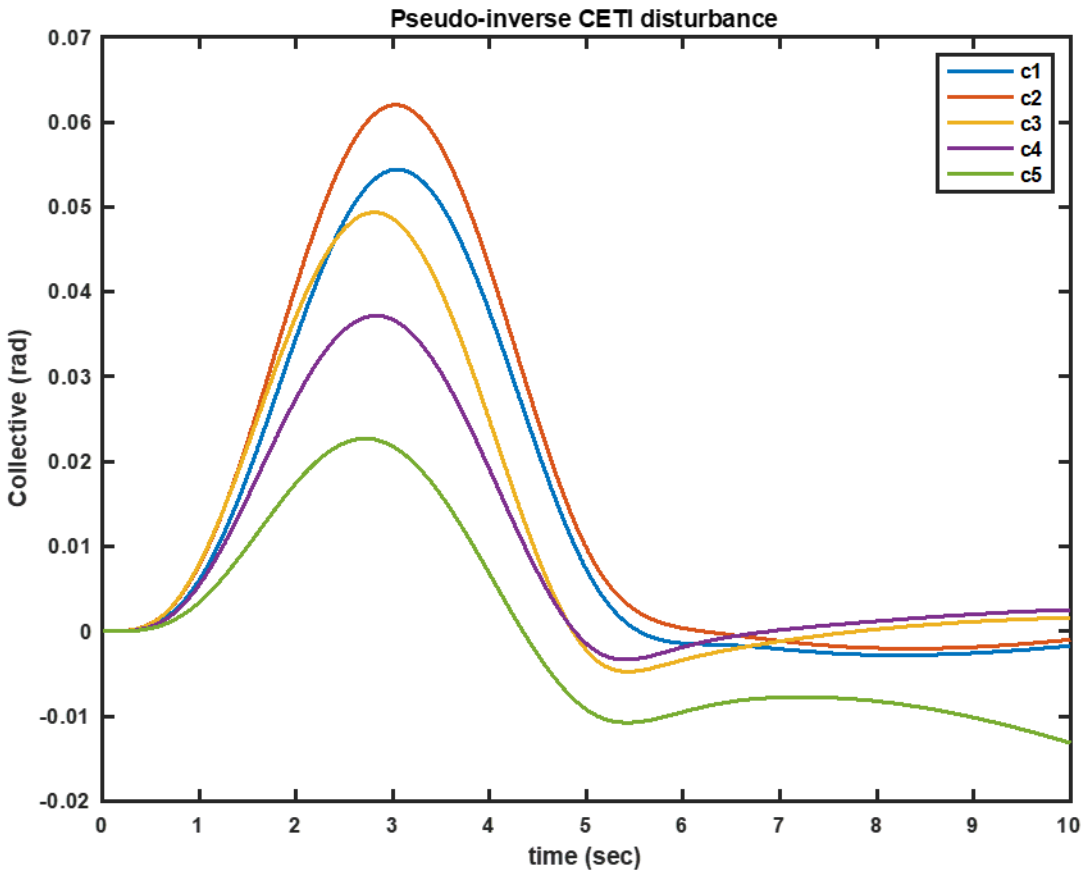

Figure 18. Control equivalent disturbance from pseudo-inverse operation on estimated perturbation accelerations

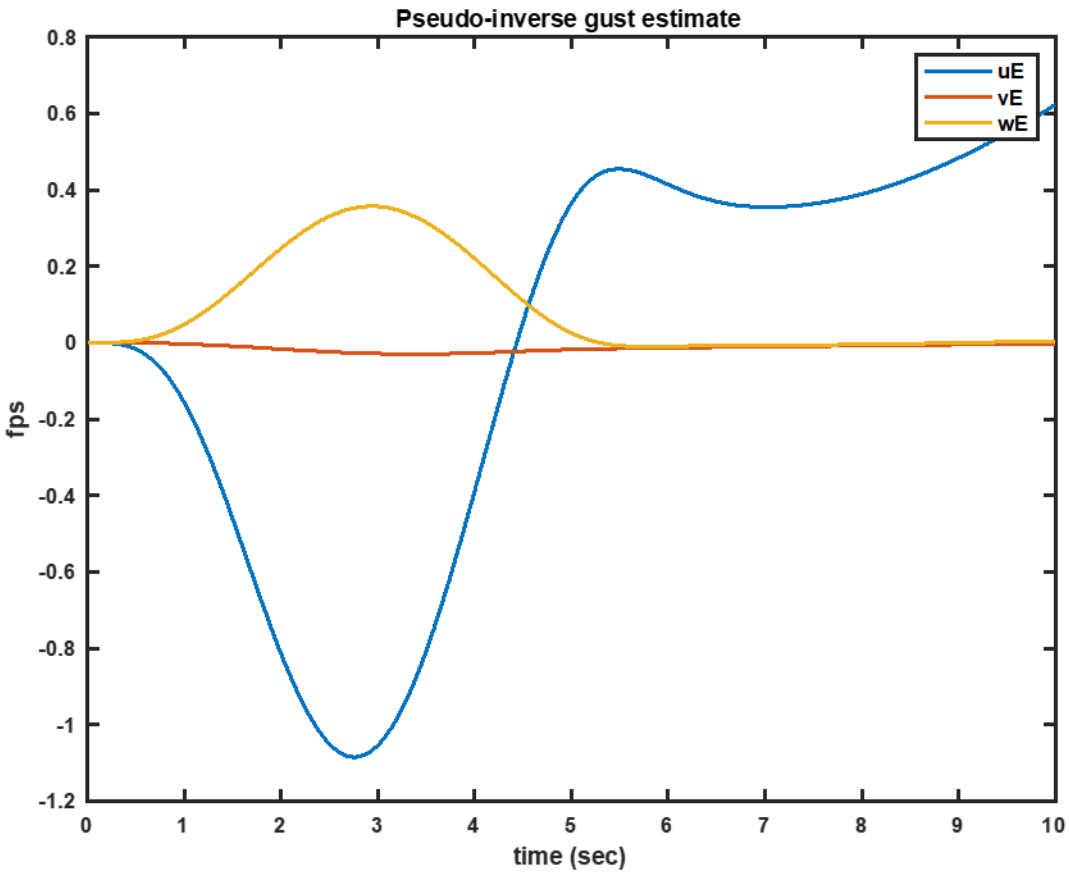

Figure 19. Estimated gust disturbances (pseudo-inverse application to acceleration perturbations)

While the estimated gust time histories from the pseudo-inverse application to the acceleration perturbations reconstructs the raised cosine input on the vertical axis, a more significant amount of gust energy is allocated to the horizontal gust estimate, (Figure 19). Both the estimated control equivalent inputs and the estimated gusts using these applications of pseudo-inverse matrices will reconstruct the estimated acceleration perturbations exactly, due to the algebraic nature of their generation from those estimates.

The DEPSim LpC aircraft model of the configuration in Figure 11 is available in various formats that include:

- a locally-linearized model with dynamic inflow for rotor wake effects,
- a locally-linearized model using the full free wake CHARM aerodynamics representation,
- an offline time-marching nonlinear model using dynamic inflow,

- an offline time-marching nonlinear model using the CHARM wake analysis,
- and a real-time nonlinear model with dynamic inflow for manned simulation applications.

The real-time nonlinear model with the CHARM wake analysis was demonstrated on graphics processing unit (GPU) machines but not yet currently ported to a manned simulation facility. We previously explored algorithm application to a lower order model of a high order linearized model of the LpC configuration. Here we apply estimation approaches on data generated from an offline time-marching CHARM-coupled simulation of the LpC configuration operating in the turbulent wake behind a hangar superstructure. This represents the test conditions used in (Lusardi, Blanken, & Tischler, 2003) for collecting data to model the spectral characteristics of control equivalent turbulence in simulation applications. The turbulent flow field (Christoffel, Hendrick, Thedin, Horn, & Schmitz, Oct. 2020) is a full boundary layer model propagated over the local building structures present at the test site, and flow velocity data was stored within a box (shown in yellow in Figure 20) on the lee side of the hangar where the UH-60 was flown.

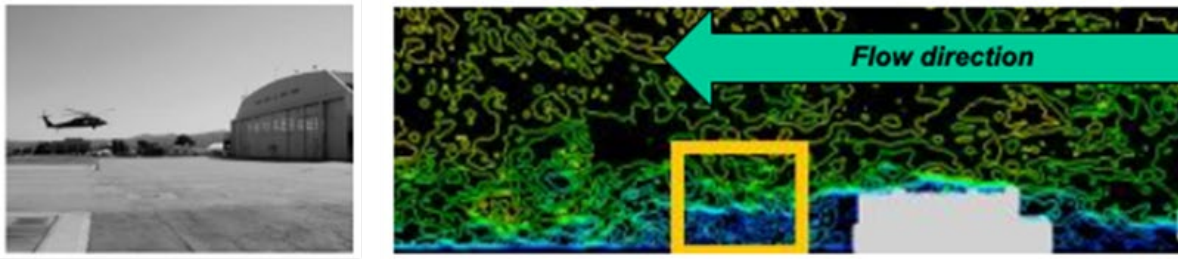

Figure 20. UH-60 CETI test condition. CFD simulation graphic of simulated turbulence

Simulation data for the LpC operating in a hover-hold condition at the same location as the UH-60 in the flight test was collected and includes the CFD effect on the CHARM vortex wake structure, along with the wake-on-wake effects seen between the different lift rotors on the vehicle. The complexity of the wake structure and the full CFD resolution of the turbulence environment make the simulation model infinite dimensional and provide an opportunity for algorithm evaluation to assess its effectiveness in estimating the gust magnitudes and statistics in the simulation from the collected response time histories.

Hover station-keeping for this simulated case shows (Figure 21) tight control of vehicle position, following an initial vertical transient of 1.5 feet from simulation initiation due to control transients.

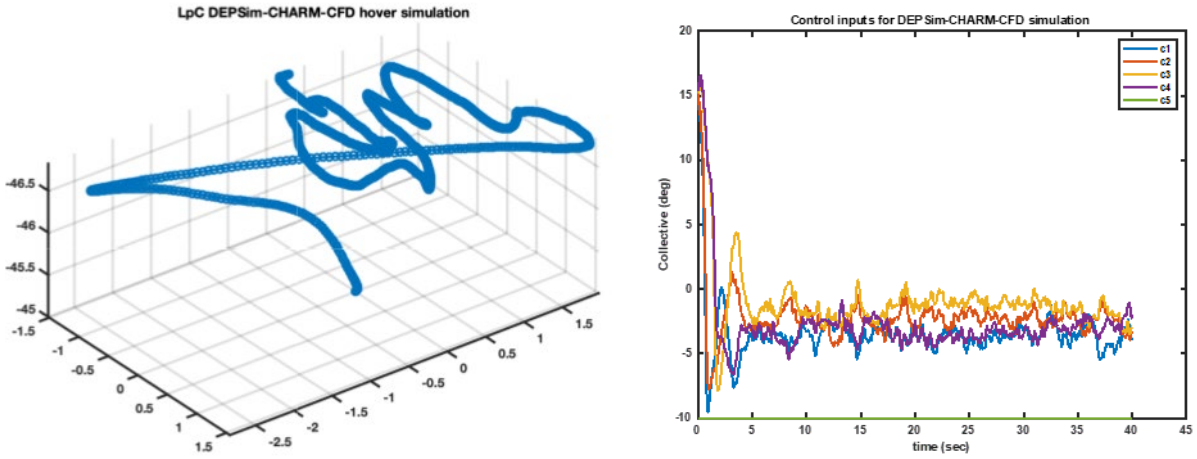

Figure 21. Inertial position and collective control history for coupled LpC simulation

Application of the state rate perturbation algorithm with pseudo-inverse equivalent control extraction and gust estimation resulted in the data shown in Figure 22, Figure 23, and Figure 24. The initial transient in the state rate perturbations had the pseudo-inverses of both the control effectiveness matrix and the gust effectiveness matrix to generate the equivalent disturbance control and the applied gust estimate. Both estimates are shown following the transient response of the filter and aircraft after 15 seconds of simulated station-keeping. While the mean of the gust estimate is close to the simulated value of 25 feet per second (fps) at that condition behind the hangar, the fluctuations in the estimate are almost a factor of two greater than that seen in the CFD data itself. This suggests that the interactional aerodynamic effects of wake-on-wake load changes generate larger force and moment perturbations on the flight vehicle than modeled with the reduced order 8 degree of freedom (DOF) representation used in the filter formulation. Note that the estimated equivalent control disturbance is relatively small, indicative of the precision hold capability of the simulated flight control system.

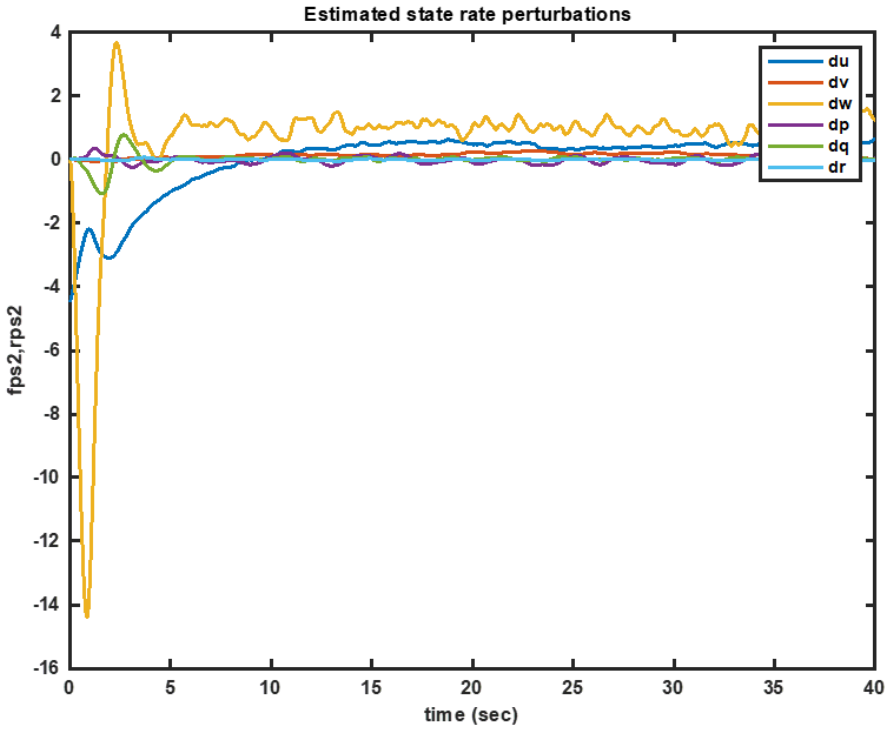

Figure 22. Estimates of state rate perturbations from the DEPSim-CHARM-CFD simulation

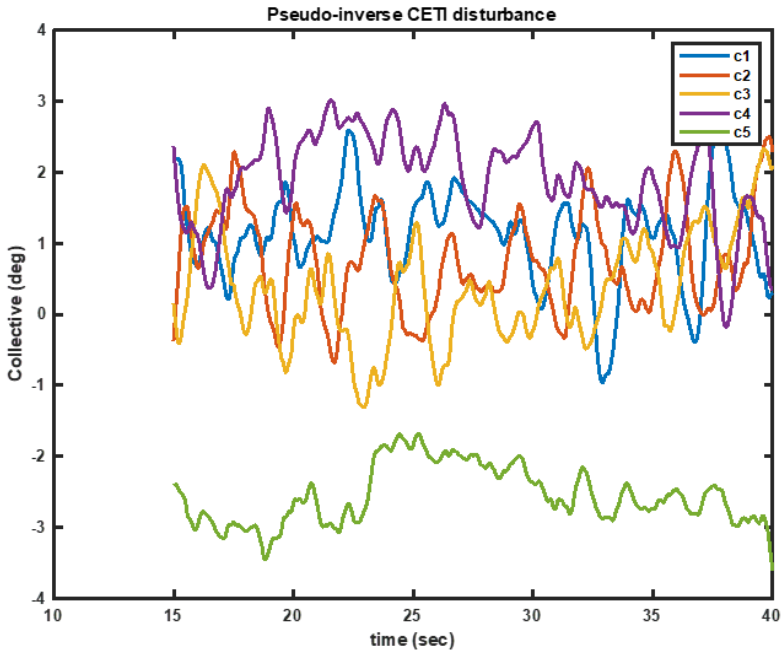

Figure 23. Estimated equivalent disturbance control inputs from coupled simulation

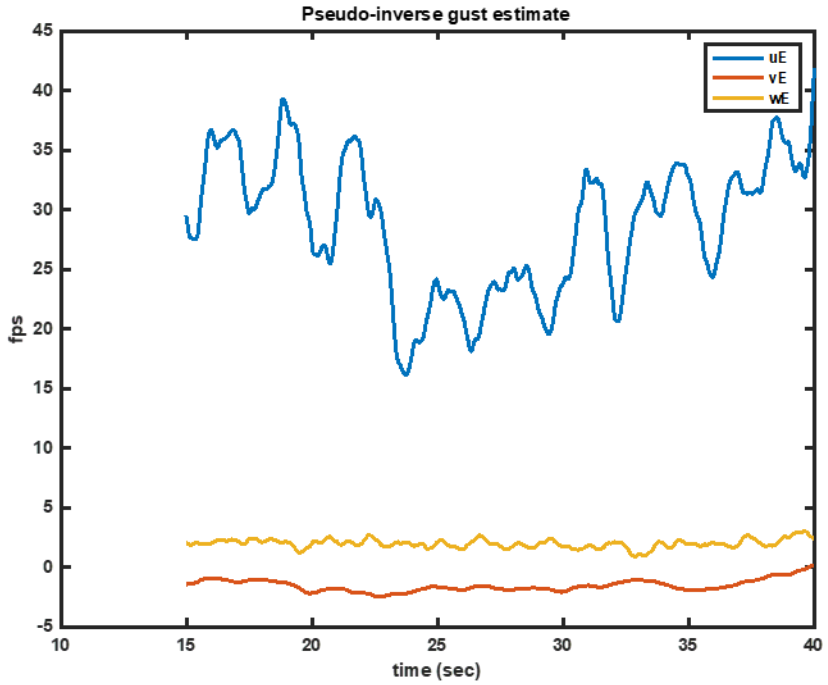

Figure 24. Estimated gust time history for DEPSim LpC in position hold simulation

The nonlinear DEPSim LpC model, having dynamic inflow wake representations for each rotor, was coupled to CDI's in-house fixed base simulation facility, as a means of evaluating both the RCP algorithm and the generation of cockpit displays of RCP during flight operations. Limited investigations were undertaken during this effort to study how best to communicate RCP information to both aircraft evaluators and pilots and to provide actionable information aiding assessment of vehicle safety. This could support certification evaluation or suggest pilot behaviors to avoid LOC-I events from saturated control channels.

A notional display of RCP for each actuator input was constructed and simulated using MATLAB graphics primitives, shown in Figure 25. The RCP limits represent ratios as defined above, and a bar extending from a neutral/center position to the current RCP value for each actuator is color coded to aid interpretation. Green indicates RCP limits below 80% of that direction's maximum input, yellow indicates values from 80% to 90%, and red indicates values 90% and over. An additional indicator is a pair of pointers in a bow-tie shape that indicates the sum of the current RCP based on the physical actuator displacement and the output-oriented RCP calculated value needed to completely null the current system disturbance. The bow-tie symbology has the same color-coding representation as the bar elements.

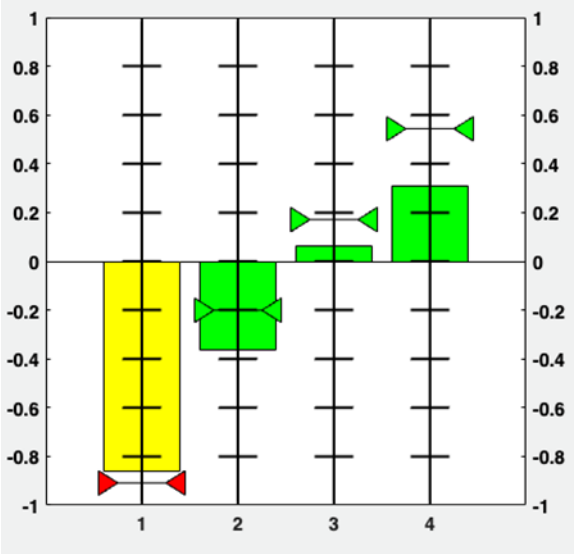

Figure 25. Notional RCP display showing input-oriented and output-oriented values

A desktop simulation of the FLIGHTCode model of the single-place quadrotor NASA concept vehicle was manually flown with this display providing readings of input-oriented RCP to understand how such information transfer might benefit pilot monitoring of limiting flight conditions. Figure 26 shows the quadrotor in flight over a cityscape with the MATLAB graphic added as an overlay window onto the 3rd-person view of the flight simulation. This limited experience guided further development of a similar display used in manned simulation trials in CDI's fixed-base simulation facility. This is shown as an integrated display window on two touchscreen monitors located in the pilot station. Figure 27 displays Java Swing graphics primitives running on a Raspberry Pi computer and interprets networked data on actuator displacements from the DEPSim simulation model.

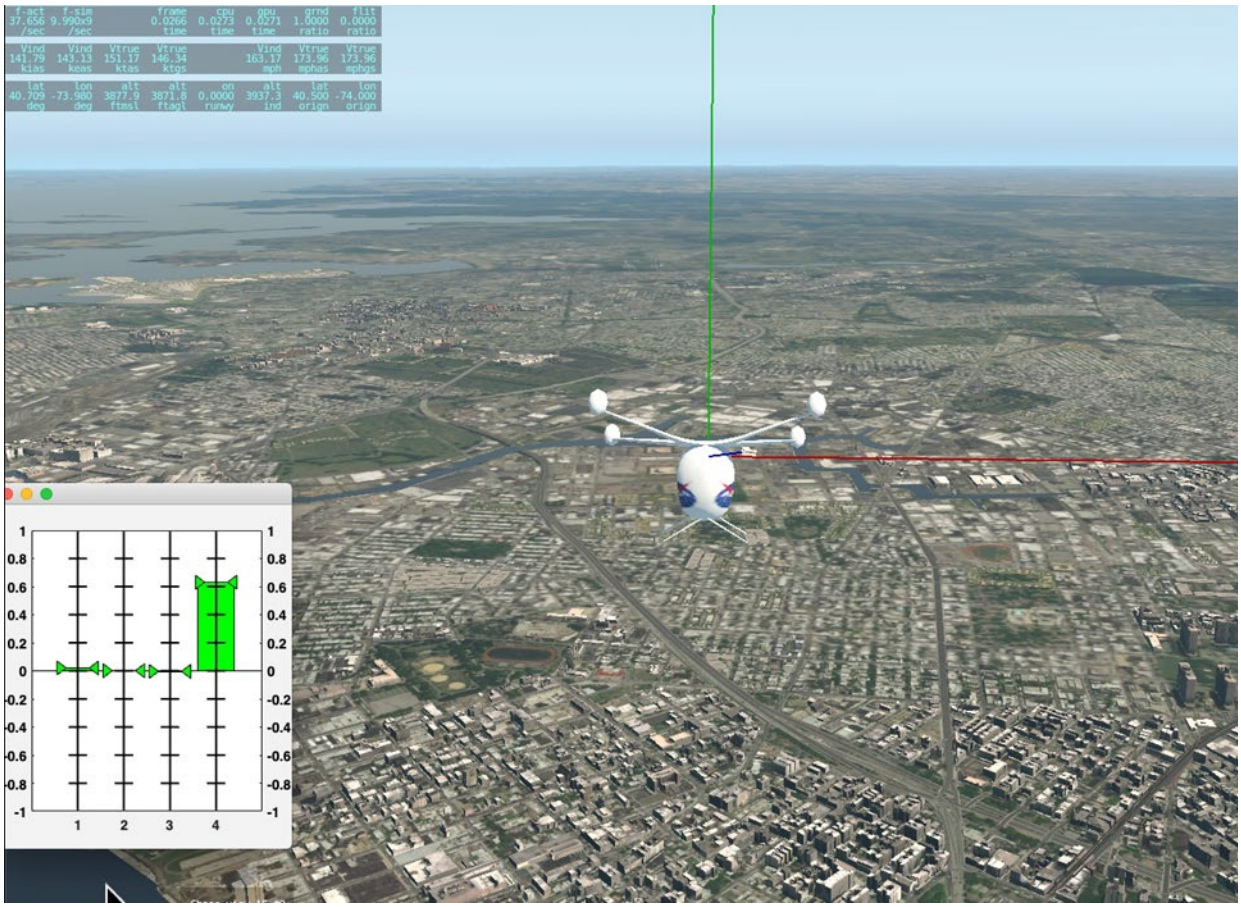

Figure 26. RCP display superimposed on NASA quadcopter flight simulation environment

Figure 27. RCP display on left cockpit monitor in CDI's fixed base simulation lab

The CDI DEPSim model was manually flown through a set of aggressive maneuvers to both evaluate the algorithm performance and to assess the utility of the linear representation of RCP values in this display format. The inertial position and lateral response rates is shown in Figure 28 from a test case to assess the control limits of the nonlinear simulation. For this simulation study, the commanded torques on the motors (Figure 29) were used in the RCP calculation process. The LpC model was a representation of the rpm-controlled (versus collective-controlled) variant of that aircraft, current limiting due to excessive rpm perturbation commands tend to limit the control capability of those DEP aircraft.

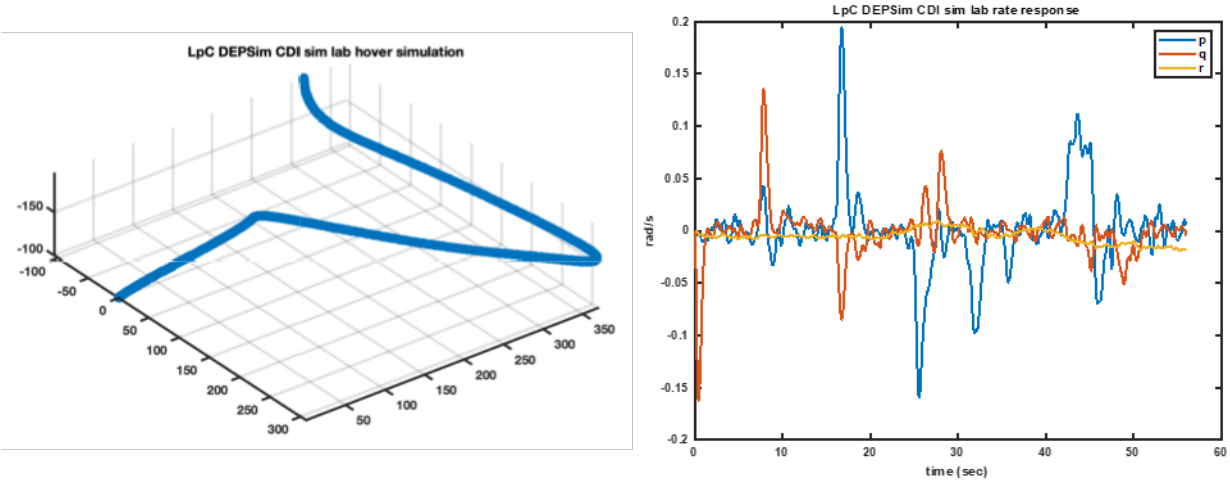

Figure 28. Spatial variation and angular rate time history for manned simulation trial event

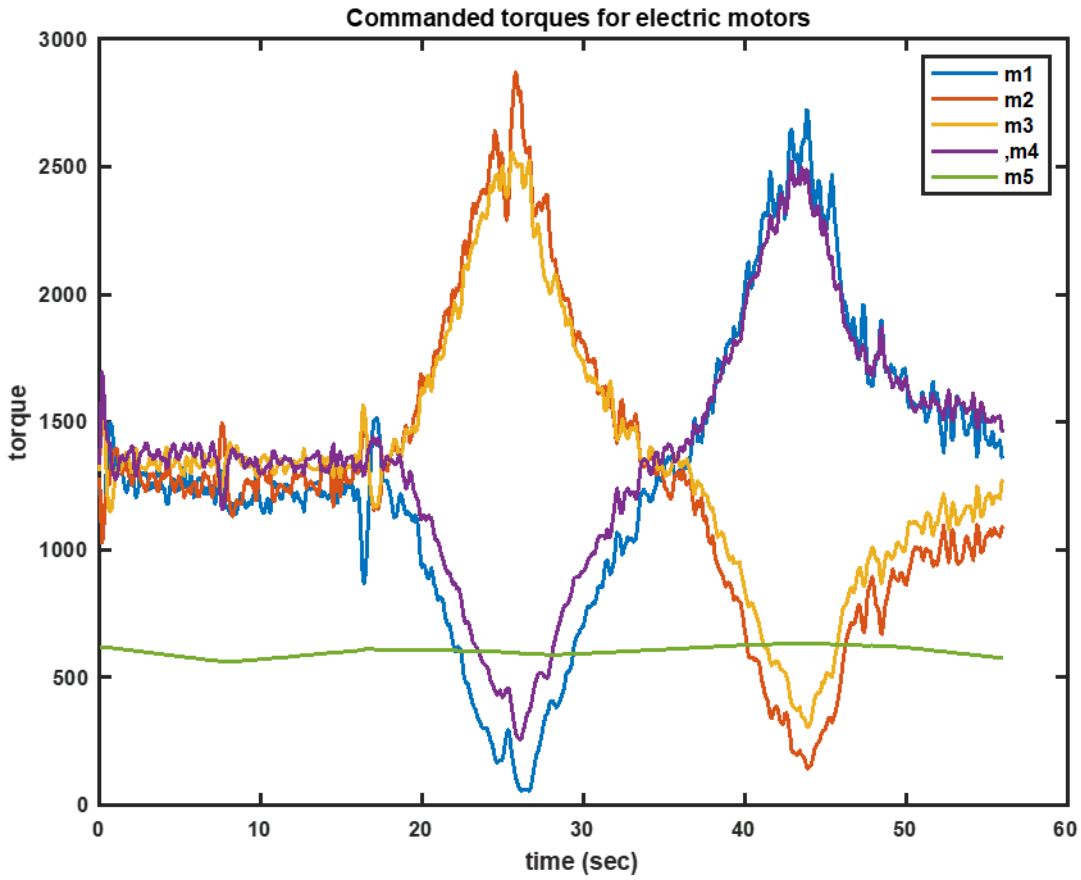

Figure 29. Torque commands for LpC lateral motion maneuver

The display of the RCP ratioed the difference of these torque commands with a nominal value of 1500 by half the maximum extent of available torque, producing a similar time history. Pilot comments on the display stated that the bars could be viewed using peripheral vision, but the indicators of output-oriented RCP were somewhat of a distraction. A suggested alternative was to eliminate them and either incorporate the output-oriented RCP directly into the bar chart display or to generate an equivalent using an estimated rate and future time prediction based on that rate. This comment suggested a modification of the input oriented RCP calculation to include a predictive component based on an average rate of control input over a preceding time interval. However, the determination of how to compute the average rate and what prediction interval is most useful remains as a future investigation in follow-on research.

5 Experimental validation

One of the tasks associated with this effort was to explore the implementation issues involved with processing flight data in real time to algorithmically determine remaining control margins and associated gust disturbance magnitudes. This demonstration work was performed on small UAV platforms that are representative of the types of control configurations present on developmental and planned eVTOL/DEP vehicles. Due to their wide commercial availability and ease of initial integration, the configuration investigated was a quadcopter. A Tarot 650 quadcopter was modified with additional instrumentation and avionics to provide a flying testbed to assess the algorithm's performance in actual turbulent conditions. Figure 30 shows the test model on a strain gauge balance with one of several three-axis anemometers used to collect turbulence measurements in the flight field where testing is taking place. Test instrumentation includes an UAV data board v5 (UDB5) open-source autopilot board that provides both inertial, GPS-derived, and control input/motor output data in a telemetry stream to a data collection and monitoring laptop computer with a real-time algorithm. This was used to determine control equivalent turbulence estimates along with gust state estimates from the telemetry frame data.

Since the quadcopter uses a model-based algorithm to extract response residuals between commanded and gust-generated flight data, it is important to properly quantify the model's response to flight (motor) commands. This response is predicted using the simulation models but can also be measured using standard system identification input-output measurements (Tischler & Remple, 2006). Control response testing on the Tarot 650 was conducted both on a static six-component sting balance and in-flight trials in calm conditions. Figure 31 shows the measured load transients from a manually generated sweep excitation of a single motor/propeller on the sting-mounted quadcopter. Figure 32 shows a vertical heave excitation of the same quadcopter while in flight. Sting balance response results provide estimates of elements within the control

effectiveness matrix (accelerations due to control inputs), while flight response measurements include vehicle motion effects (e.g., damping derivatives) to identify the vehicle system dynamics matrix elements.

Figure 30. Instrumented Tarot 650 on sting balance with 3-axis anemometry stand

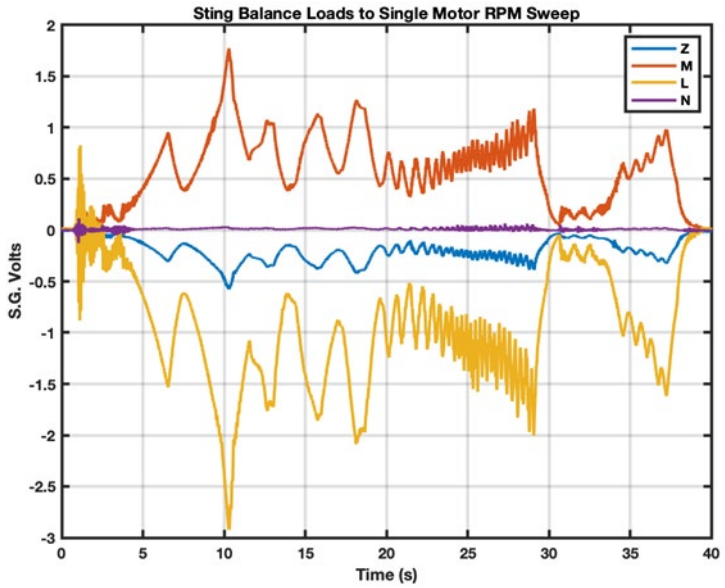

Figure 31. Sting balance time history for single rotor frequency sweep

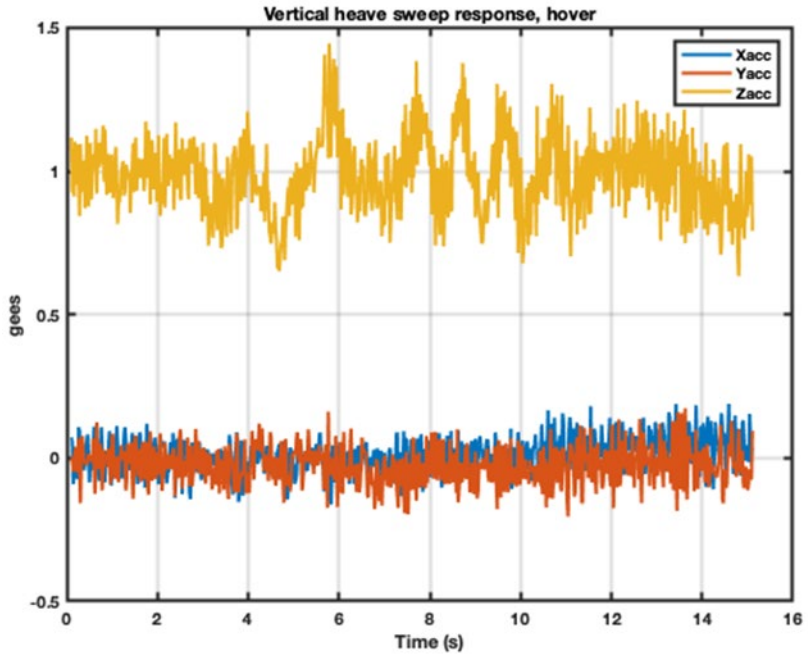

Figure 32. Vertical heave frequency sweep acceleration response, hover

Instrumentation for this first series of UAV tests required a somewhat hybrid approach, as the recommended core autopilot for the Tarot 650 was used for vehicle stabilization but represents a "black box" since measured data from its internal IMU/magnetometer/GPS instrumentation is not available to the operator. The command signals to the individual motor controllers were routed to the UDB5 board via Y-connectors, and individual optical sensors were installed to collect motor rpm data on each arm. The on-board six-axis IMU (three gyros, three accelerometers) and a separate patch GPS antenna and integral processor completed the measurement arrangement. A schematic of the installed avionics for this test is shown in Figure 33. Note that this instrumentation complement is both minimal and does not interfere with the on-board autopilot used for platform stabilization. In fact, if the data from the autopilot sensors and command signals to the motor controllers were made available, only the serialization and telemetry link would be required as additional avionics for conducting this test.

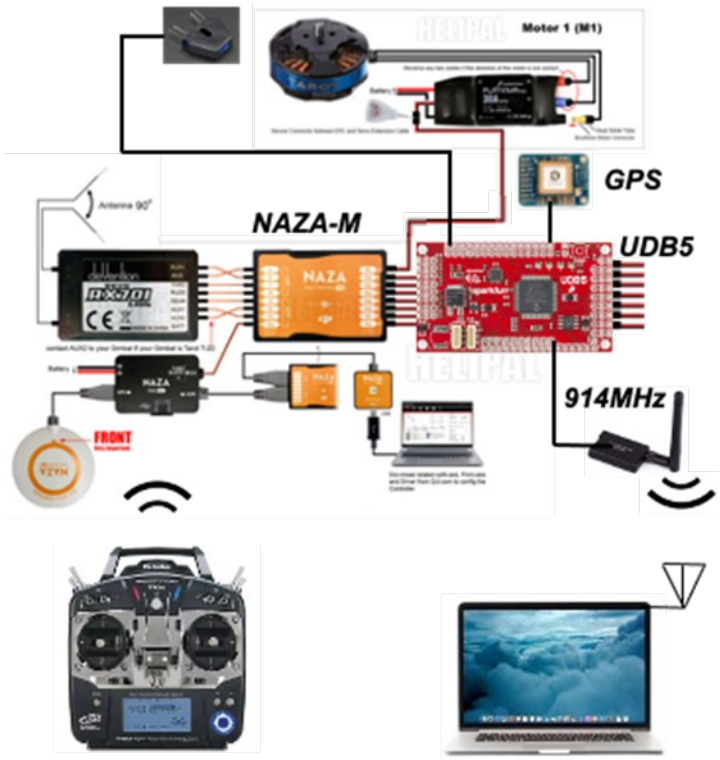

Figure 33. Tarot 650 quadcopter avionics with added test instrumentation

5.1 Disturbance flight testing

Evaluation of the algorithm is ideally determined if the estimated gust disturbance from vehicle response measurements is what is present at the current vehicle location. This implies that the disturbance environment is known, or at a minimum, its statistics (mean and variance) is quantified over the area of flight operations. Initial plans for UAV testing in the exhaust flow area of the FAA's Airflow Induction Test Facility at the William Hughes Tech Center at Atlantic City, NJ were shelved when that facility underwent refurbishment, and instead free-flight testing was conducted north of the airport itself.

A B-737 aircraft with functional engines is located near an access road north of Atlantic City International Airport (KACY), as seen in Figure 34 and exhausts into a flat triangular field having low brush and minimal vegetation. It was used as a surrogate controlled gust environment for disturbance testing of the quadcopter. Since the maximum forward speed of the Tarot 650 is approximately 45 mph, the starboard engine was operated at idle thrust throughout the testing activity. Two tests on separate days were conducted at this site, with the first a hover condition in the jet flow, and a second with a translation through the shear layer of the jet exhaust.

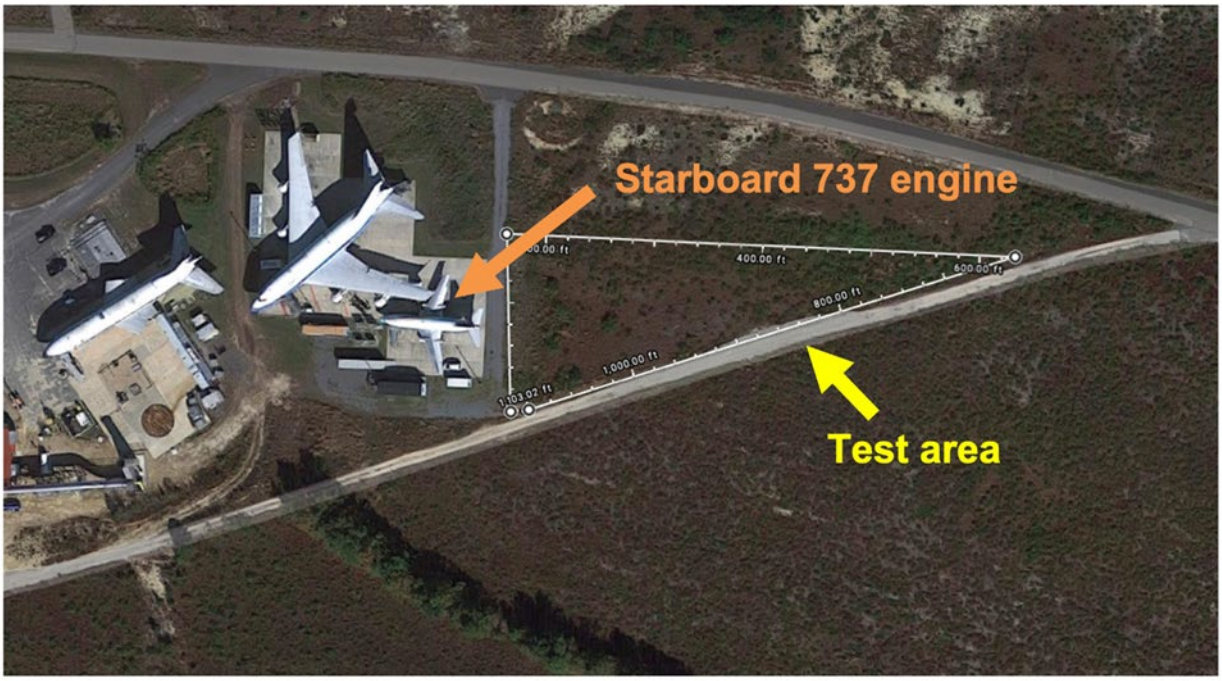

Figure 34. Quadcopter test site (white triangle) behind B-737 engine north of KACY

A three-axis anemometer was placed at several locations behind the jet flow to collect mean and variance data on the disturbance flow environment. A custom data collection package was used with user real-time display to digitize and store the anemometer data onto a memory card within a Raspberry Pi single board computer, attached to the anemometer array. For the second sortie, the instrumented quadcopter was flown into and out from the exhaust flow to excite the vehicle response, separate from the pilot controls or autopilot stabilization commands driving the four lift motors.

Data was collected throughout the flight trials and monitored on a laptop collecting telemetry over a 940MHz serial data link. Video and still recording of the flight were collected for use in event reconstruction from the telemetry traces. A still image from the flight through the jet exhaust is shown in Figure 35, and the trajectory of the flight paths (12/07/21 in green, and 12/14/21 in blue) from the onboard GPS updates is given in Figure 36.

Figure 35. Quadcopter in transition behind B-737 exhaust flow

Figure 36. Quadcopter flight paths for both sorties (hover and transition)

The hover flight tests were conducted at a conservative distance from the B-737 jet exhaust from a location directly in line with the starboard engine. Control of hover was maintained within the disturbance, with stabilizations commands occasionally reaching limits for the associated motor controller. As all flight activity was within the jet exhaust, no definitive change in general character of the measured response and associated remaining control power metric was observed. The second sortie on 12/14/21 was planned to have the quadcopter encounter both the jet blast

and ambient wind conditions in a flight across the location of the jet flow, providing a known change in flow disturbance that would exercise the algorithm's potential for detection of changes in remaining control power.

Figure 37 shows stacked time histories from the transition flight, which started within the jet exhaust flow, transitioning out of the exhaust field, and then returning to and passing the initial takeoff location. The plot shows computed values of RCP for the forward (#2) rotor of the quadcopter, along with the GPS velocity, pitch rate, and vertical accelerometer from that flight. The quadcopter experiences the jet blast shortly after liftoff (at 80s), but then transitions further north of the jet flow into relatively benign conditions (at 115s). The high frequency excitation of the quadcopter pitch response while operating in the jet exhaust is evident in the vertical acceleration trace over the approximately 35s operation within the jet flow. This is reflected in the frequent minimum values in the RCP metric for the motor as the autopilot attempts to mitigate this disturbance. Once the quadcopter is clear of the jet blast, the nominal values of RCP increase above those while within the jet turbulence, despite the maneuvering flight used to return to the takeoff location. When the quadcopter encounters the jet blast again, at a higher altitude, actual LOC was experienced (near 142s), and the quadcopter pitched forward and sped past the launch location, requiring flight termination. These preliminary results show that the simplified algorithm using only control effector limits has a likelihood of providing useful measurements of remaining control power based on the correlation between this metric and the telemetry and observed vehicle behavior in this test.

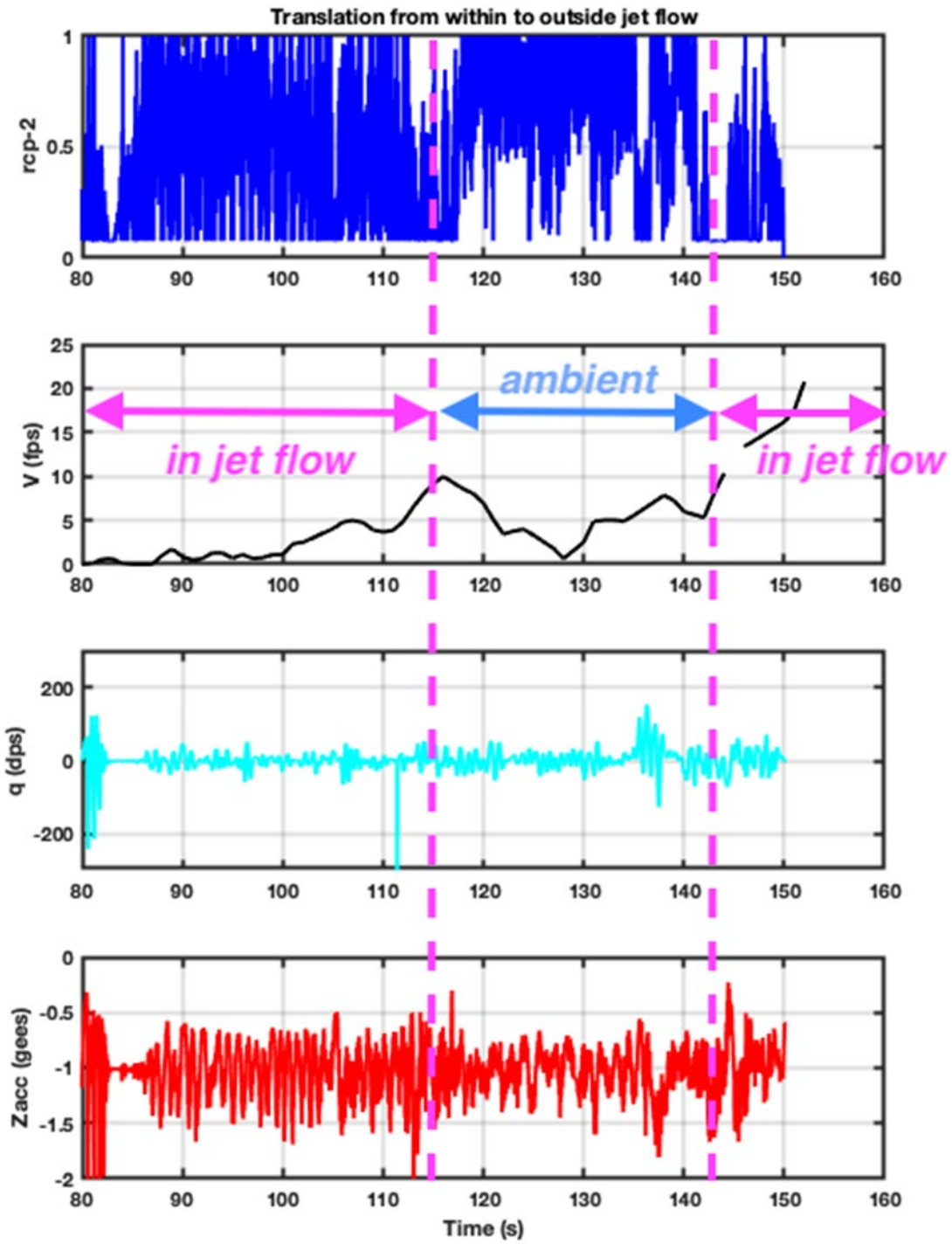

Figure 37. Computed RCP from telemetry during quadcopter transition flight test

5.2 Measured control effectiveness

Initial results from examination of input-oriented RCP estimation appear promising in the determination of incipient LOC-I events, based on this quadcopter test. However, it is of interest to assess the predictive capability of output-oriented RCP estimation, and the direct estimation of gust inputs, using this same data set. Since both estimation algorithms depend upon a recursive filter operating on measured versus predicted vehicle response based on a math model of the aircraft control effectiveness, these data were also applied to determine what that effectiveness was during the flight tests. This approach used a simplified algebraic relationship between control perturbations and differences in vehicle accelerations to determine this relationship. This is like the pseudo-inverse approach used to estimate perturbation rates from the lower-order dynamic model. A variant of this technique is used in the control design approach embodied in Incremental Nonlinear Dynamic Inversion.

Flight test measurements from the quadcopter tests revealed that the isolation mounts on the UDB5 board were transferring high frequencies to the sensor, making direct time history evaluation of this relationship problematic. However, conversion to frequency domain representation shows the relationship quite clearly. Figure 38 shows the frequency response of the pitch command pulse width signal to the pitch rate from the UDB5 board, displaying a significant trend line at low frequency of a pure differentiation, or a direct moment input response to this control command. Similar such representations are used to extract these coefficients in the control effectiveness matrix to permit mapping of control input to vehicle rate response if vehicle system models are lacking or presumed in error.

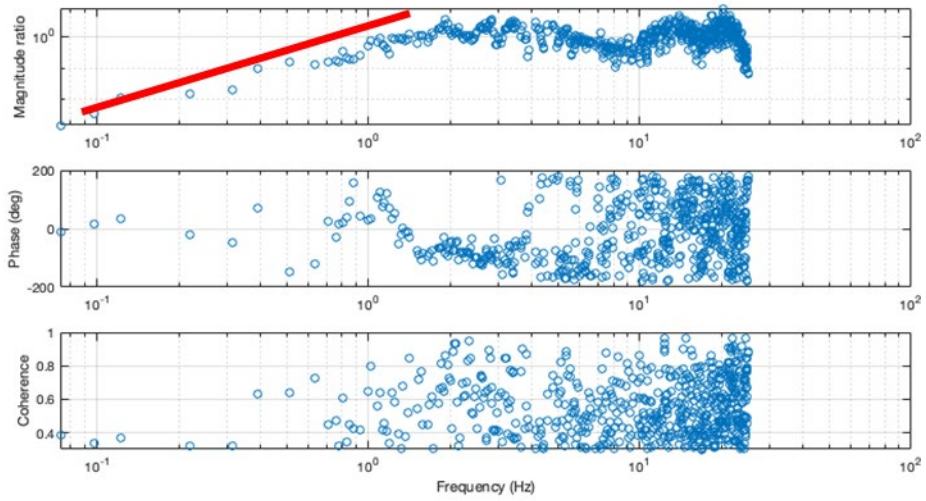

Figure 38. Frequency response of pitch command PWM to pitch rate from flight test

Follow-on flight testing was planned to incorporate components from the Tarot 650 quadcopter with a commercially available electric airplane with pusher propeller to represent a lift plus cruise configuration like that used in the above algorithm analysis. However, the fabricator and test pilot for this effort, Mr. Marty Zeller, passed away suddenly during the execution of this research program. His contribution to this effort and his enthusiastic and warm support are appreciated by all who encountered him.

6 Conclusions

This research shows that the application of algorithms for estimating remaining available vehicle control power, and local gust disturbance magnitudes, appear to provide a usable safety assessment for avoiding LOC events for eVTOL/DEP aircraft. Such real-time safety metrics may aid the challenge of providing safety assurance in certification of these aircraft for operations within the national airspace system. The algorithms have several notable features which ease their implementation for use in aircraft certification testing, or on-board monitoring for safety assurance that include:

- The input-oriented RCP estimation and the output-oriented gust disturbance and RCP estimation schemes are completely flight control system agnostic, as they only incorporate measurements associated with the base functionality of the aircraft.
- Methods for combining recursive estimation of both gust disturbances and equivalent control disturbances have shown to be compatible through pseudo-inverse mapping of estimated perturbations in vehicle state rates from those commanded from control inputs.
- Low-order models of aircraft response are appropriate for estimating RCP as they fall within the frequency range of both atmospheric disturbances and handling qualities for these eVTOL/DEP vehicles.
- Recursive estimation of both gust disturbances and RCP includes Gaussian statistics that can further impact the assessment of possible vehicle LOC-I events during flight, providing an additional margin of safety.

Future work using these algorithms could investigate their applicability to other configurations of eVTOL/DEP aircraft, as well as conventional rotorcraft and fixed-wing aircraft, both piloted and uncrewed.

7 References

Christoffel, T., Hendrick, C., Thedin, R., Horn, J., & Schmitz, S. (Oct. 2020). Towards Validation of a Dynamic Interface Simulation using Flight Test Data. *VFS 76th Annual Forum.* Virtual.

Johnson, W., Silva, C., & Solis, E. (2018). Concept Vehicles for VTOL Air Taxi Operations. *Aeromechanics Design for Transformative Vertical Flight.* San Francisco, CA: AHS.

List, A., & Hansman, R. J. (2019). *Assessing Multi-rotor UAV Controllability in Low Altitude Fine-Scale Wind Fields.* Cambridge, MA: M.I.T. International Center for Air Transportation.

Lusardi, J., Blanken, C., & Tischler, M. (2003). Piloted Evaluation of a UH-60 Mixer Equivalent Turbulence Simulation Model. *59th AHS Annual Forum.* Phoenix, AZ.

McConville, A., Richardson, R., & Moradi, P. (2022). Comparison of Multirotor Wind Estimation Techniques Through Conventional On-board Sensors. *AIAA SciTech Forum.* San Diego, CA.

McKillip, J. R. (2018). *Real-time Turbulence Recognition and Reporting System for Unmanned Systems.* Ewing, NJ: CDI Report 18-10, for Navy SBIR Contract N68335-18-C-0348.

McKillip, J. R., & Keller, J. (2021). *Development of a Rotorcraft Flight Dynamics and Control Modeling and Analysis Tool for Conceptual Design: FlightCODE Theory Manual.* Ewing, NJ: CDI Technical Note 2108.

McKillip, J. R., Keller, J., & Kaufman, A. (2002). Algorithmic Icing Detection for the V-22 Osprey. *Flight Controls and Crew System Design Specialists Meeting.* Philadelphia, PA: AHS.

McKillip, J. R., Keller, J., Wachspress, D., Whitehouse, G., & Quackenbush, T. (2010). Simulation of Dynamic Interface Flight Control Concepts Using the CHARM Toolbox for MATLAB. *Specialists Conf. on Aeromechanics.* San Francisco, CA: AHS.

McKillip, R. (2018). *Real-time Turbulence Recognition and Reporting System for Unmanned Systems.* Ewing, NJ: CDI Report 18-10, for Navy SBIR Contract N68335-18-C-0348.

Seher-Weiss, S., & von Gruenhagen, W. (2009). Development of EC 135 Turbulence Models via System Identification. *35th European Rotorcraft Forum.* Hamburg, Germany.

Stoll, A. a. (2022). Transition Performance of Tilt Propeller Aircraft. *VFS 78th Annual Forum.* Ft. Worth, TX.

Theron, J., Horn, J., & Wachspress, D. (2020). An Integrated Simulation Tool for eVTOL Aeromechanics and Flight Control. *Aeromechanics for Advanced Vertical Flight Technical Meeting.* San Jose, CA: VFS.

Tischler, M., & Remple, R. (2006). *Aircraft and Rotorcraft System Identification, 2nd Ed.* Reston, VA: AIAA.

Tobias, E., & Tischler, M. (2016). *A Model Stitching Architecture for Continuous Full Flight-Envelope Simulation of Fixed-Wing Aircraft and Rotorcraft from Discrete-Point Linear Models.* U.S. Army RDECOM Special Report RDMR-AF-16-01.

Withrow-Maser, S., Malpica, C., & Nagami, K. (2020). Multirotor Configuration Trades Informed by Handling Qualities for Urban Air Mobility Application. *VFS 76th Annual Forum.* Virtual: Vertical Flight Society.